

## Title page

# Aripiprazole cytotoxicity coincides with activation of the unfolded protein response in human hepatic cells

## Authors:

Francesca Forno<sup>1</sup>, Yossi Maatuf<sup>1</sup>, Shatha Boukeileh<sup>1</sup>, Priya Dipta<sup>1</sup>, Mohamed Mahameed<sup>1</sup>, Odai Darawshi<sup>1</sup>, Vitor Ferreira<sup>2,3</sup>, Patricia Rada<sup>2,3</sup>, Irma García-Martínez<sup>2,3</sup>, Einav Gross<sup>4</sup>, Avi Priel<sup>1</sup>, Ángela M. Valverde<sup>2,3</sup>, Boaz Tirosh<sup>1</sup>

## Affiliations:

<sup>1</sup>Institute for Drug Research, School of Pharmacy, Faculty of Medicine, Hebrew University of Jerusalem, Jerusalem, Israel

<sup>2</sup>Instituto de Investigaciones Biomédicas Alberto Sols (CSIC-UAM), 28029, Madrid, Spain

<sup>3</sup>Centro de Investigación Biomédica en Red de Diabetes y Enfermedades Metabólicas Asociadas (CIBERdem), ISCIII, 28029, Madrid, Spain

<sup>4</sup>Dept. of Biochemistry and Molecular Biology, IMRIC, Faculty of Medicine, The Hebrew University of Jerusalem, Ein Kerem. P.O. Box 12271, Jerusalem, 9112102, Israel

JPET# 264481

Running title page

Aripiprazole induces the UPR in liver cells

Correspondence to: Boaz Tirosh, The School of Pharmacy, The Hebrew University of Jerusalem, POB 12065, Jerusalem 91120, Israel. e-mail [boazt@ekmd.huji.ac.il](mailto:boazt@ekmd.huji.ac.il), Tel. +972-2-6758730, Fax +972-2-6758741

Number of text pages: 17

Number of tables: 0

Number of figures: 6

Number of references: 37

The number of words in the Abstract: 250

The number of words in the introduction: 750

The number of words in the discussion: 1156

Abbreviations: Ari, Aripiprazole; CYP3A4, cytochrome P450 3A4; DMSO, Dimethyl sulfoxide; ER, endoplasmic reticulum; FFAs, free fatty acids; MEL 526, melanoma cells; U87, glioblastoma cells; NAC, N-acetyl L-cysteine; Ola, Olanzapine; PI, propidium iodide; ROS, reactive oxygen species; SGA, second generation of antipsychotics; Tg, thapsigargin; Tm, Tunicamycin; UPR, unfolded protein response; XBP1s, transcription factors spliced XBP1.

Recommended section: cellular and molecular

## Abstract

Schizophrenia is a mental disease that results in decreased life expectancy and wellbeing, by promoting obesity and sedentary lifestyles. Schizophrenia is treated by antipsychotic drugs. While the second generation of antipsychotics (SGA), Olanzapine and Aripiprazole are more effective in treating schizophrenia, they display a higher risk of metabolic side effects, mostly by development of diabetes and insulin resistance, weight gain as well as dyslipidemia. Endoplasmic reticulum (ER) stress is induced when ER homeostasis of lipid biosynthesis and protein folding is impaired. This leads to the activation of the unfolded protein response (UPR), a signaling cascade that aims to restore ER homeostasis or initiate cell death. Chronic conditions of ER stress in the liver are associated with diabetes and perturbed lipid metabolism. These metabolic dysfunctions resemble the pharmacological side effects of SGAs. We, therefore, investigated whether SGAs promote the UPR in human and mouse hepatocytes. We observed full-fledged activation of ER stress by Aripiprazole, not by Olanzapine. This occurred at low micromolar concentrations and to variable intensities in different cell types, such as hepatocellular carcinoma, melanoma and glioblastoma. Mechanistically, Aripiprazole caused depletion of ER calcium, leading to activation of IRE1 and PERK, two major transducers of the UPR. Cells underwent apoptosis upon Aripiprazole treatment, which coincided with UPR induction, and this effect was reduced by adding glutathione without affecting UPR itself. Deletion of IRE1 from HepG2 cells protected cells from Aripiprazole toxicity. Our study reveals for the first time a cytotoxic effect of Aripiprazole that involves the induction of ER stress.

## Significance statement

The anti-schizophrenic drug Aripiprazole exerts cytotoxic properties at high concentrations. This study shows that this cytotoxicity is associated with the induction of endoplasmic reticulum (ER) stress and IRE1 activation, mechanisms involved in diet-induced obesity. Aripiprazole induced ER stress and calcium mobilization from the ER in human and mouse hepatocytes. Our study highlights a new mechanism of Aripiprazole that is not related to its effect on dopamine signaling.

## Introduction

Schizophrenia is a worldwide mental disease that results in decreased life expectancy, association with obesity and sedentary lifestyle. It affects around 0.3%-0.7% of the population at young ages, although in certain cases it can appear in a later stage of life (van Os and Kapur, 2009). Schizophrenia typically occurs during late adolescence and early adulthood and is characterized by abnormal social behavior. Common symptoms are false beliefs, unclear or confused thinking and hearing imaginary voices. The causes of schizophrenia are assumed to be a combination of genetic and environmental factors (Owen et al., 2016). From a genetic point of view, the heritability is around 80%, although environmental factors such as living environment, drug abuse and prenatal stress also contribute to its etiopathogenesis (van Os and Kapur, 2009).

Aripiprazole (Ari) and Olanzapine (Ola), drugs of the latest generation of antipsychotics, referred to as second generation anti-schizophrenics (SGAs), have shown high efficacy to treat this mental disorder. However, they display a greater risk of metabolic side effects (i.e., weight gain, dyslipidemia and type 2 diabetes). The mechanisms responsible for these severe metabolic disturbance are still unknown. Some studies suggest that hypothalamic dopamine antagonism or disruption of hypothalamic regulation of glucose levels, along with anticholinergic-induced inhibition of insulin secretion, could play a role (Panariello et al., 2011). However, peripheral effects of the drugs that are unrelated to their dopamine antagonism or effects in the central nervous system were also invoked.

The endoplasmic reticulum (ER) is the entry point into the secretory system in which proteins acquire their folded state and assemble into complexes. ER stress occurs when the amount of protein entering the ER exceeds its folding capacity. This imbalance induces an adaptive reaction collectively termed the unfolded protein response (UPR) (Frakes and Dillin, 2017). The mammalian UPR is transduced by three major ER sensors, IRE1, PERK, and ATF6 that undergo activation under ER stress conditions. When unfolded proteins accumulate at the ER, the chaperone GRP78 dissociates from the sensors and allows their activation (Amin-Wetzel et al., 2017). IRE1 and PERK are activated by autophosphorylation, while ATF6 traffics to the Golgi. Activated IRE1 splices the mRNA of XBP1 in a non-canonical fashion, yielding the potent transcription factor spliced XBP1 (XBP1s) (Yoshida et al., 2001). Activated PERK phosphorylates eIF2 $\alpha$ , which causes the attenuation of global protein synthesis. At the same time, selective translation of certain mRNA molecules such as ATF4 is induced. ATF6 is proteolytically fragmented in the Golgi yielding an active transcription factor (Ye et al., 2000). Whereas acute ER stress leads to apoptosis, chronic sub-lethal ER stress causes cellular adaptation and resistance to apoptosis, characterized by modulation of mRNA localization and stability (Rutkowski et al., 2006). The UPR profoundly affects cellular homeostasis, regulating cell cycle, apoptosis, metabolism and autophagy. Studies in animal models have demonstrated that extended activation of the UPR plays an important role in chronic metabolic diseases, including obesity, insulin resistance, and diabetes (Ozcan et al., 2004). Specifically, obesity may be a consequence of chronic ER stress, particularly in the liver and adipose tissues. Part of the mechanism is the role of UPR in promoting inflammatory conditions (Liu et al., 2016). In this regard, all three main branches of the UPR mediate cell autonomous pro-inflammatory

transcriptional programs, which are mainly governed by transcription factors such as NF- $\kappa$ B and AP-1 (Hotamisligil and Erbay, 2008; Verfaillie et al., 2013). The signaling pathways involved in the UPR and inflammation are interconnected through various mechanisms, including the production of reactive oxygen species (ROS) and the release of calcium from the ER (Zhang and Kaufman, 2008), as well as direct stimulation of the secretion of pro-inflammatory cytokines. Interestingly, free fatty acids (FFAs), which are elevated in obesity, have the potential to induce ER stress in various cells, including adipocytes and hepatocytes (Jiao et al., 2011; Cnop et al., 2012; Pardo et al., 2015).

Owing to the connection of ER stress and obesity, we explored whether SGA drugs induce ER stress. We observed full-fledged activation of the UPR at low micromolar concentrations of Ari, but not of Ola in hepatic cells. This was associated with cell death and was rescued in part by inhibition of IRE1, or the addition of reduced glutathione. Our data indicate a previously unknown pharmacological activity of Ari in inducing ER stress conditions and UPR signaling. It should be noted that the concentrations that induce the UPR in cultured cells are approximately 25 fold higher than the pharmacokinetic  $C_{\max}$  of Ari under its regular dosing regimen, suggesting that this pharmacodynamic property may be related more to Ari over dosage toxicity. However, the exact exposure of the liver to Ari, particularly following oral administration is not known.

## Material and Methods

### Experimental procedures

#### Cell lines and culture conditions

HepG2, Hep3B, Mel 526 and U87 cells were cultured in high glucose Dulbecco's Modified Eagle medium (DMEM high glucose, Sigma-Aldrich) supplemented with 10% fetal bovine serum (FBS, Invitrogen), 2 mM L-glutamine (Biological Industries, Israel), 1% penicillin–streptomycin solution (Biological Industries, Israel), and 1 mM sodium pyruvate (Biological Industries, Israel). Cells were incubated at 37 °C under 5% CO<sub>2</sub>.

#### Chemical reagents

Aripiprazole (Acros Organics #129722-12-9), Olanzapine (Sigma-Aldrich #035M4781V), Rifampicin (Apollo #AS470050), Z-VAD(OMe)-FMK (Cayman chemical #0542527-4), N-acetyl-L-cysteine (Sigma-Aldrich#616-91-1), BAPTA-AM (ThermoFisher #B6769), EGTA (Sigma-Aldrich #67-42-5), STF-083010 (Tocris Bioscience #1A/213103 ), Glutathione reduced ethyl ester (Sigma-Aldrich #92614-59-0) propidium iodide (Sigma-Aldrich #25535-16-4), GSK2606414 (TOCRIS #5107), Thapsigargin (Fermentek #67526-95-8), Tunicamycin (Fermentek #11089-65-9) and DMSO (Biosolve #044075).

#### Western blotting

Cells were either trypsinized or directly harvested by cell scraping, centrifuged at 3,000 rcf for 5 min, and washed twice in cold PBS. For cell lysis, RIPA buffer supplemented with protease and phosphatase inhibitors was added in a volume of about four times of the cells pellet and then vibrated for 20 min at 4 °C. Lysates were cleared by centrifugation at 20,000 rcf for 30 min at 4 °C. Protein content was measured by BCA. Reduced Laemmli sample buffer (5X) was added, boiled for 5 min at 95 °C, and loaded on SDS-PAGE. Following SDS-PAGE, gels were blotted onto PVDF membranes using BioRad PowerPac™. Blots were blocked in 10% skim milk in TBST buffer for 1 h at room temperature. The following primary antibodies were used: rabbit anti-PERK (1:1000) (Cell Signaling #5683); rabbit anti-IRE1 antibody (1:1000) (Cell Signaling #3294S); rabbit anti-phospho IRE1 (S724) antibody (1:1000) (Abcam #ab124945); mouse anti-puromycin antibody, clone 12D10 (1:1000) (Millipore #MABE343); polyclonal rabbit anti-p97 (1:5000) was provided by Dr. Ariel Stanhill (Open University, Israel). Secondary HRP-conjugated goat anti-rabbit and anti-mouse (Jackson ImmunoResearch, West Grove, PA) were used. Blots were developed in Bio-Rad ChemiDoc™ XR. Quantification was done by densitometry by using Image Lab™ software.

#### Quantitative Real-Time PCR (qPCR) and analysis of XBP1 mRNA splicing.

Total RNA was isolated using TRI-reagent (Bio-Rad Laboratories, Berkeley, CA). cDNA was synthesized using 1 µg RNA with qScript™ cDNA Synthesis KIT (Quanta Biosciences, Beverly, MA) according to the manufacturer's instructions. Bio-Rad iTaq™ universal SYBR® Green Supermix was used for qPCR analyses. Actin was used as an endogenous housekeeping

gene for PCR quantification. Analysis was performed on CFX Connect™ Real-Time PCR Detection System (Bio-Rad) using the Bio-Rad CFX manager 3.1 software. The following primers were used: CYP3A4: forward- 5'-TGAAGTTCATCTGCACCACCG-3', reverse- 5'-AGTCGTGCTGCTTCATGTGGT-3'; Actin forward- 5'-CCAACTACTTCCTTAAGATCATCCAAC-3', reverse- 5'-ACATGCGGATCTGCTGCA-3'. RT-PCR was used for the detection of XBP1 mRNA splicing using 5× Red Load Taq (LAROVA) with forward- 5'-CCTTGTAATTGAGAACCAGG-3', reverse- 5'-CCAAAAGGATATCAGACTCGG-3'.

#### Puromycin labeling for protein synthesis evaluation

Cells were harvested, centrifuged, and resuspended in 3 ml of fresh medium. A portion of 1 ml was analyzed for cell counts and the remaining 2 ml were pulsed for 10 min by adding 10 µl of puromycin solution (Millipore; cat #508838; 10 mg/ml). Following the addition of puromycin, cells were immediately incubated at 37°C under mild shaking, and ice-cold PBS was added to a volume of 40 ml to terminate the protein labeling. Cells were washed twice with cold PBS. 10×10<sup>6</sup> cells, according to the count analysis performed, were then lysed in 200 µl of 1× reduced Laemmli sample buffer preheated to 70°C. Equal volumes were loaded on 12% SDS-PAGE and probed with an anti-puromycin antibody following blotting.

#### Live cell calcium imaging

Cells were spotted onto glass coverslips coated with Poly D-Lysine (PDL) and allowed to settle down for 2.5 h at 37°C and 5% CO<sub>2</sub>. Cells were loaded with 2.5 µM Fura-2-AM dissolved in Ringer solution (mM): 150 NaCl, 2.5 KCl, 1.8 CaCl<sub>2</sub>, 1 MgSO<sub>4</sub>, 10 HEPES and 10 D-glucose, adjusted to pH 7.4 with NaOH and supplemented with Pluronic F-127 acid (0.02%), for 1h at RT in the dark. Cells were washed twice with Ringer solution and then illuminated with a 175 W xenon arc lamp, and excitation wavelength (340/380 nm) were selected by a Lambda DG-4 monochromatic wavelength changer. Intracellular calcium concentration was measured by digital video microfluorometry with a front-illuminated interline CCD camera using MetaFluor Fluorescence Ratio Imaging Software. Dual images (340 and 380 nm excitation, 510 nm emission) were collected, and pseudocolor ratio-metric images were monitored every 4 s during the experiment. All the experiments were conducted at room temperature.

#### Generation of knock-out cells using CRISPR/Cas9

gRNA was designed according to Doench *et al.* and cloned into PX459 vector according to the Zhang lab protocols (Doench *et al.*, 2016). HepG2 cells were transfected using Transit 2020 (3 µl per 1 µg DNA, Mirus Bio, Madison, WI) and then underwent puromycin selection (2 µg/ml) for 48 h followed by single-cell cloning by limiting dilution. Clones were screened by immunoblotting for the target protein. gRNA sequences for human PERK: 5'-CCGAGGCTCCTGCTCTCCCG-3'; 5'-GAATATAACCGAAGTTCAAAG-3', gRNA sequences for human IRE1: 5'-CTTTTATGTCTGGCAGCGGG-3'.

#### Flow cytometry

JPET# 264481

Cells were harvested, centrifuged, and washed twice in PBS, filtered through a 100  $\mu$ M strainer directly to FACS tubes. Analyses were performed with Cytoflex cytometer (Beckman Coulter, Brea, CA) using the CytExpert software.

#### Propidium iodide staining

To evaluate the percentage of dead cells using flow cytometry analysis, 1  $\mu$ l of propidium iodide (1 mg/ml) was added to the cells before the analysis. Equal number of events were recorded, and PE positive cells were gated and considered as dead cells.

#### Isolation and culture of primary mouse hepatocytes

Mice received health care according to Spanish and European legislation. All animal experimentation was approved by the CSIC and Comunidad de Madrid Animal Care and Use Committees. Primary mouse hepatocytes were isolated from 8-10 week old male C57Bl6 mice by perfusion with collagenase as described (Benveniste *et al.*, 1988). Cells were seeded on 6 or 12-well collagen IV pre-coated plates (Corning, New York, NY) and cultured in media containing DMEM and Ham's F-12 medium (1:1) supplemented with heat-inactivated 10% FBS, 2 mM glutamine, 15 mM glucose and 1 mM sodium pyruvate (attachment media). Cells were maintained in this medium for 24 h. Then, the medium was replaced with fresh media containing the indicated drugs.

#### Oil Red-O and Hematoxylin & Eosin staining

Hematoxylin & Eosin and Oil Red-O staining was performed as previously reported (Erez *et al.*, 2017).

## Results

### Aripiprazole at low micromolar concentration induces ER stress

The peak plasma concentration of Ari in treated patients typically reaches 1-2  $\mu\text{M}$  concentration under chronic regimen (Nagai et al., 2017). However, the corresponding concentrations of the drug in the liver can be much higher. For example, Ola levels in the liver of rats are 30 fold higher than that of the serum levels (Aravagiri et al., 1999). Although we have not found documentation on Ari concentrations in the liver or serum in rodents, we assume that high  $\mu\text{M}$  to low mM concentrations may represent a reasonable exposure to the liver at the clinical dosage regimen. Treatment of the human HCC cell line HepG2 with increasing concentrations of Ari showed that IRE1 was hyperphosphorylated at concentrations higher than 20  $\mu\text{M}$  (**Fig. 1A and B**). The SERCA inhibitor thapsigargin (Tg) was used as a positive control for UPR induction. Moreover, the total level of IRE1 was induced by Ari, a typical effect of ER stress (Shemorry et al., 2019). We detected phosphorylated IRE1 as early as 4h after Ari addition (**Fig. 1C**). This was accompanied by the splicing of XBP1 mRNA. (**Fig. 1A, lower panel**). Immunoblotting analysis of PERK showed the shift pattern in its electromobility upon stress (Tg and Ari), which is due to its auto-phosphorylation (**Fig. 1A**). This mobility shift was not observed by co-incubation with the PERK inhibitor (**supplemental figure 1**), thus both arms of the UPR are activated by Ari. These data are supported by the analysis of newly synthesized proteins which indicate a concentration-dependent reduction by Ari, a feature of eIF2 $\alpha$  phosphorylation by PERK (**supplemental figure 2, panels A and B**).

Ola and Ari affect schizophrenia in similar mechanisms by curtailing dopamine signaling. However, Ola did not induce the UPR at concentrations up to 50 $\mu\text{M}$  (**Fig. 1D**). This suggests that the mechanisms by which Ari activates the UPR may not be related to dopamine signaling. To exclude a relationship of Ari-mediated UPR and the activation of dopamine receptors, we treated the HepG2 cells with a combination of Ari and dopamine. Dopamine alone neither promoted the UPR nor inhibited UPR induction by Ari (**supplemental figure 2, panel C**).

We treated a second HCC cell line, Hep3B, to explore whether the ER stress caused by Ari is a general effect of the drug. We observed an even stronger induction of ER stress in this line (**supplemental figure 3, panel A**). Ari, though to a less extent, also promoted ER stress in melanoma (MEL526) and glioblastoma cells (U87), indicating that this is a general pharmacological response to the drug. The fact that Ari induces ER stress in specialized drug-metabolizing cells, such as liver cells, and in non-drug metabolizing cells, suggests that drug metabolism is not required for UPR induction. To address this, we treated Hep3B cells with the cytochrome P450 3A4 (CYP3A4) inducer rifampicin and compared the induction of the UPR. While CYP3A4 mRNA was induced by rifampicin as expected, we did not observe differences in UPR induction (**supplemental figure 3, panel B**), indicating that Ari-mediated induction of the UPR is independent of drug catabolism.

### Aripiprazole induces calcium mobilization from the ER

ER homeostasis is perturbed by several insults such as depletion of calcium content, a metal ion essential for chaperone activity and protein folding at mM concentrations. Once calcium

leaks to the cytoplasm, protein folding is inhibited and UPR is induced. We performed live cell calcium imaging in HepG2 cells following an overnight treatment to test whether ER calcium levels are affected by Ari. The experiment was design in a manner that after the overnight treatment, the remaining calcium in the ER is released by Tg treatment in the course imaging (**Fig. 2A**). Thus, a positive signal indicates levels of ER calcium concentration. As expected, DMSO (negative control) provided the highest signal while Tg overnight treatment (positive control) completely dwindled the calcium storage in the ER resulting in no effect of Tg in the course of imaging. Similar to Tg, which depleted the storages of calcium in the ER when added overnight, Ari used at concentrations above 20  $\mu$ M resulted in the diminishing of calcium levels in the ER (**Fig. 2B**). We challenged Hep3B cells with 30  $\mu$ M concentration to generalize the effect of Ari on calcium mobilization. We observed that calcium ER was mobilized in these cells as well (**supplemental figure 3, panels D and E**). The dose response correlation of ER calcium mobilization and the induction of the UPR reflect a causative relationship, indicating that Ari induces the UPR by causing calcium depletion from the ER.

### Aripiprazole cytotoxicity is regulated by the UPR

The UPR is an adaptive response to ER stress that promotes survival, a response termed “adaptive UPR”. However, it also participates in induction of apoptosis if the stress is not resolved, termed as the “terminal UPR” (Hetz et al., 2015). The transition between adaptive to terminal UPR is dependent on the stressor and the cell type. Cytotoxicity of Ari has been previously demonstrated, but the mechanism is not well understood and was postulated to involve inhibition of tyrosine kinases, such as SRC and Syk (Kim et al., 2018b; Yoo et al., 2018). In dopaminergic neurons, Ari protected from glutamate-induced cytotoxicity. The dual activities of Ari may suggest that, similar to the UPR, it controls pro-survival and pro-death programs. We, therefore, investigated whether at concentrations that UPR is induced, Ari exerts a cytotoxic effect. **Fig. 1** shows mild ER stress in HepG2 cells at 20  $\mu$ M, and its intensity increases in a concentration dependent manner up to 30  $\mu$ M. However, at concentrations higher than 30  $\mu$ M, very little cells survived after 24 h treatment (**supplemental figure 4**). At first, we verified whether the mechanism of Ari-mediated cell death is caspase-dependent. Cell death was evaluated by flow cytometry, examining light scattering properties and positive staining of dead cells with propidium iodide (PI). Inclusion of the pan caspase inhibitor ZVAD-FMK inhibited Ari toxicity when used at 30  $\mu$ M concentration (**Fig. 3B**). To examine whether the UPR plays a role in the cytotoxicity of Ari, we generated IRE1 KO and PERK KO HepG2 cells by CRISPR/Cas9 gene editing (**supplemental figure 5, panel A**). Again, cells were treated overnight with 30  $\mu$ M Ari. As shown in **Fig. 3A**, deletion of PERK mildly reduced the number of dead cells although with no statistical significance, while IRE1 deletion significantly protected the cells against death (**Fig. 3A**). This effect was also supported in melanoma cells treated with an IRE1 inhibitor (**supplemental figure 3, panel B**). Altogether, these data indicate that while both arms of the UPR may participate in Ari cytotoxicity, IRE1 seems to play a dominant role. Unfortunately, we were unable to address ATF6 contribution due to the absence of specific inhibitors to this UPR arm as well as specific antibodies.

### Glutathione protects cellular viability downstream to the UPR

ER stress and particularly calcium leakage from the ER induce reactive oxygen species (ROS) production (Cao and Kaufman, 2014). Conversely, oxidative stress promotes ER stress by affecting the process of protein folding. To obtain better insight into this interaction in the context of Ari toxicity, we treated HepG2 cells with ROS and calcium scavengers and assessed viability by flow cytometry. It should be noted that the addition of DMSO as the vehicle control resulted in 2-7% of cell death, a variability probably associated with culture conditions. We thus normalized the cell death in each experiment to that of its own DMSO control. The addition of N-acetyl L-cysteine (NAC) and the calcium chelators BAPTA and EGTA did not reduce the cytotoxicity of Ari in HepG2 cells (**Fig. 4**). In fact, BAPTA and EGTA were toxic by themselves (**supplemental figure 7, panel B**). However, when reduced glutathione (GSH) was added using GSH ethyl ester, we observed a significant improvement in survival of the cells relative to Ari alone (**Fig. 5**). Under these conditions, UPR activity was not affected (**supplemental figure 6**) suggesting that glutathione protects cell viability by mechanisms that are either downstream or independent of the UPR.

### **Aripiprazole induces the UPR, lipid accumulation and calcium mobilization from the ER in primary mouse hepatocytes**

We isolated primary hepatocytes from mouse livers and treated them with Ari at different concentrations for different time periods to examine if Ari elicits ER stress in untransformed hepatocytes. Tunicamycin (Tm) was used as a positive control for UPR induction. **Fig. 6A** illustrates Ari-induced UPR as early as 4 h upon addition to primary mouse hepatocytes as indicated by IRE1 and PERK phosphorylation and the splicing of XBP1 mRNA (**Fig. 6A-E**). Analysis of ER calcium in the primary hepatocytes confirmed its depletion by Ari, as was observed in human HCC cells (**Fig. 6, G and H**). This also occurred at concentrations lower than 20  $\mu$ M. In contrast to HCC cells, Ari-induced UPR in the primary cells was maintained till 12 h of treatment and then it was reduced (not shown), suggesting that primary hepatocytes are able to adapt to this stress. However, the viability of the primary hepatocytes was compromised after 24 h of treatment (**supplemental figure 8, panel C**). Interestingly, oil-red-o positive lipid droplets were visualized in the surviving cells (**Fig. 6F**). These data suggest that in contrast to transformed cells, which die by apoptosis, primary hepatocytes adapt to Ari-induced ER stress, and the adaptation involves accumulation of intracellular lipids. To demonstrate a connection between Ari-induced UPR and the accumulation of intracellular lipids, we performed a dose-response analysis. To avoid artifacts of cell death, we limited the incubation to 12 h and elevated the concentration of Ari up to 40  $\mu$ M. Lipids accumulated in association with the development of UPR, assayed by XBP1 mRNA splicing (**supplemental figure 8, panels A and B**). These data are consistent with the induction of liver steatosis by Ari reported in rats (Soliman et al., 2013). Evidence of ER stress was not observed *in vivo* following a single administration of Ari at a dose of up to 50 mg/kg in mice (data not shown). It is noteworthy to mention that solubilization of the drug was not achieved in a mixture of Tween-80, DMSO and water, and the drug was eventually administered as a suspension.

## Discussion

Stress responses evolved to respond to transient insults and protect the hosts until stress conditions dissipate. However, if stress lingers in a chronic manner, adaptation may involve irreversible plasticity that ultimately affects tissue function and leads to pathology. As such, chronic conditions of ER stress have been implicated in metabolic and inflammatory diseases in a manner that cannot be reversed even if the stress eventually subsides. Congruent with this hypothesis is the difficulty to identify the initial mechanisms associated with drug induced liver injuries. In some cases, following exposure to the drug even for a short duration, pathological conditions develop in a manner that cannot be reversed upon cessation of the drug treatment. Typical examples are amiodarone- and tamoxifen-induced liver steatosis. For amiodarone we have previously showed that ER stress can be the initial trigger for the steatosis following a single administration of the drug (Erez et al., 2017).

The development of weight gain, insulin resistance, diabetes and dyslipidemia in SGAs treated patients is a clinical problem worldwide that limits compliance. The molecular mechanisms underlying these metabolic changes may be subtle and short-lived. Thus, stress responses triggered by SGAs are a plausible mechanism for the side effects developed in patients treated with these drugs. With this premise we sought to test whether Ari and Ola induce ER stress and UPR signaling. Although Ola treatment is more prone to induce metabolic derangement and weight gain in patients with schizophrenia than Ari (Musil et al., 2015), we found that Ari, but not Ola, induces ER stress as evident by the UPR signaling (Fig. 1). A second difference between Ari and Ola relates to cytotoxicity. While Ari *in vitro* is toxic at low micromolar concentrations, Ola at this concentration range is not toxic. This suggests that the two drugs have fundamental pharmacodynamic properties that are not related to their effects in dopamine signaling.

Most likely the induction of ER stress by Ari occurred by the parental drug in all cell lines tested in a dopamine receptor-independent manner (**supplemental figures 2 and 3**). These results indicate a new off-target effect of Ari that may occur during treatment when its concentrations in the liver exceed the threshold for adaptive UPR. Our data clearly show that ARI-induced ER stress correlates with calcium mobilization from the ER (**Fig. 2**), but it is unclear which mechanisms mediate this response. Calcium homeostasis in the ER is controlled by its active transport to the ER by SERCA, its leakage through the Sec61 translocon (Lang et al., 2017), or by triggering ionotropic calcium channels such as the IP3R (Taylor and Tovey, 2010). Thus, further investigation is needed to delineate which of these mediators of the ER machinery are responsible for the depletion of calcium induced by Ari.

The cytotoxicity of Ari has been documented for several cancer cell lines (Baek et al., 2015; Kim et al., 2018b; Yoo et al., 2018). Some studies suggested that Ari inhibits key tyrosine kinases of the SRC family as the mechanism responsible of cell death (Kim et al., 2018b). While this mechanism has not been addressed in our study, assessment of the contribution of the different molecular pathways to Ari-induced cell death is rather complex. Our data confirm the cytotoxic properties of Ari (**Fig. 3 and supplemental figure 4**). In particular, in HepG2 cells death was associated with ER stress, suggesting a correlation between both phenomena.

Apoptosis induced by ER stress is a complex process that is modulated by the UPR itself. Each branch of the UPR has been shown to be implicated in promoting both viability and cell death. This is largely dependent on the magnitude of the stressor and the cell type. In fact, IRE1, primarily by XBP1-independent mechanisms, promotes cell death (Maurel et al., 2014). Curiously, it is also implicated in promoting survival of several tumor types (Tang et al., 2014). Likewise, PERK also promotes cell death by enhancing CHOP levels and elevating ROS production (Zeeshan et al., 2016). However, PERK is also a potent oncogene in certain tumors and confers protection against certain chemotherapies (Luo and Lee, 2013; Ju et al., 2017). At least for HepG2 cells, removal of IRE1 circumvents Ari-induced cell death (Fig. 3A). We have not investigated further downstream mediators responsible for this effect and, in this regard, further research is needed. Removal of IRE1 results in hyperactivation of PERK and ATF6 pathways, therefore the mechanism of protection seen in IRE1 KO may be PERK-dependent. Preliminary data show that the protective effect of IRE1 deletion is partially lost in IRE1/PERK double KO HepG2 cells (results not shown), supporting a role for PERK in promoting survival rather than death of HepG2 cells in the absence of IRE1. Since both IRE1 and PERK are druggable, we investigated whether pharmacological inhibition of IRE1 can protect from Ari-induced cell death. Inhibitors for IRE1 are being developed for cancer and diabetes (McGrath et al., 2018), which include inhibitors to both kinase and RNAase activities of the protein. While the effect of IRE1 RNAse inhibitor in HepG2 cells was minor, in melanoma cells it protected from Ari-induced cell death. These data may provide a novel indication for IRE1 inhibitors and should be explored in animal models.

Since ER and oxidative stress are intimately connected, to further investigate the mechanisms of cell death induced by Ari we analyzed whether calcium chelators or elevating the reductive potential of the cells may offer protection. Both EGTA and BAPTA-AM were toxic to HepG2 cells, thus we could not establish calcium leakage as the reason for cell death. However, addition of NAC at low mM concentration did not affect HepG2 viability. A possible explanation for such lack of effect could be the inability to change the redox balance at this time-frame. We did observe a mild protective effect for reduced glutathione when added directly, however cells were still susceptible to Ari-induced cell death (**Fig. 5**). UPR induction by Ari was not affected by GSH addition, suggesting that depletion of GSH is not an upstream trigger for ER stress, and its restoration improves the cellular fitness to curtail Ari cytotoxicity in an ER stress-independent manner.

While cancerous cell lines responded to Ari by triggering ER stress resulting in cell death, primary hepatocytes responded to Ari with much faster kinetics of stress induction and accumulation of intracellular lipids. The pro-lipogenic effect of Ari in primary hepatocytes is consistent with the *in vivo* effect of Ari in human and rodents. While there is little evidence of liver damage following of Ari treatment in the clinics, increased incidence of liver steatosis has been reported for Ari and other SGAs treated patients (Morlan-Coarasa et al., 2016). Since ER stress induced genetically or by overexpression of misfolded proteins is also involved in liver steatosis (Kim et al., 2018a), Ari-mediated ER stress should be further investigated primarily in individuals who already suffer from indolent non-alcoholic liver diseases with no apparent

JPET# 264481

symptoms. Our work suggests that these patients should be carefully monitored when treated with SGAs.

#### Authorship contributions

Participated in research design: Boaz Tirosh, Francesca Forno, Ángela M. Valverde, Avi Priel, Einav Gross.

Conducted experiments: Francesca Forno, Yossi Maatuf, Shatha Boukeileh, Vitor Ferreira Patricia Rada, Irma García-Martinez.

Performed data analysis: Francesca Forno, Yossi Maatuf, Priya Dipta, Mohamed Mahameed, Odai Darawshi.

Wrote or contributed to the writing of the manuscript: Boaz Tirosh, Francesca Forno, Ángela M. Valverde, Avi Priel, Einav Gross.

## References

- Amin-Wetzel N, Saunders RA, Kamphuis MJ, Rato C, Preissler S, Harding HP and Ron D (2017) A J-Protein Co-chaperone Recruits BiP to Monomerize IRE1 and Repress the Unfolded Protein Response. *Cell* **171**:1625-1637 e1613.
- Aravagiri M, Teper Y and Marder SR (1999) Pharmacokinetics and tissue distribution of olanzapine in rats. *Biopharm Drug Dispos* **20**:369-377.
- Baek KS, Ahn S, Lee J, Kim JH, Kim HG, Kim E, Kim JH, Sung NY, Yang S, Kim MS, Hong S, Kim JH and Cho JY (2015) Immunotoxicological Effects of Aripiprazole: In vivo and In vitro Studies. *Korean J Physiol Pharmacol* **19**:365-372.
- Cao SS and Kaufman RJ (2014) Endoplasmic reticulum stress and oxidative stress in cell fate decision and human disease. *Antioxid Redox Signal* **21**:396-413.
- Cnop M, Foufelle F and Velloso LA (2012) Endoplasmic reticulum stress, obesity and diabetes. *Trends Mol Med* **18**:59-68.
- Doench JG, Fusi N, Sullender M, Hegde M, Vaimberg EW, Donovan KF, Smith I, Tothova Z, Wilen C, Orchard R, Virgin HW, Listgarten J and Root DE (2016) Optimized sgRNA design to maximize activity and minimize off-target effects of CRISPR-Cas9. *Nat Biotechnol* **34**:184-191.
- Erez N, Hubel E, Avraham R, Cohen R, Fishman S, Bantel H, Manns M, Tirosh B, Zvibel I and Shibolet O (2017) Hepatic Amiodarone Lipotoxicity Is Ameliorated by Genetic and Pharmacological Inhibition of Endoplasmic Reticulum Stress. *Toxicol Sci* **159**:402-412.
- Frakes AE and Dillin A (2017) The UPR(ER): Sensor and Coordinator of Organismal Homeostasis. *Mol Cell* **66**:761-771.
- Hetz C, Chevet E and Oakes SA (2015) Proteostasis control by the unfolded protein response. *Nat Cell Biol* **17**:829-838.
- Hotamisligil GS and Erbay E (2008) Nutrient sensing and inflammation in metabolic diseases. *Nat Rev Immunol* **8**:923-934.
- Jiao P, Ma J, Feng B, Zhang H, Diehl JA, Chin YE, Yan W and Xu H (2011) FFA-induced adipocyte inflammation and insulin resistance: involvement of ER stress and IKKbeta pathways. *Obesity (Silver Spring)* **19**:483-491.
- Ju SM, Jo YS, Jeon YM, Pae HO, Kang DG, Lee HS, Bae JS and Jeon BH (2017) Phosphorylation of eIF2alpha suppresses cisplatin-induced p53 activation and apoptosis by attenuating oxidative stress via ATF4-mediated HO-1 expression in human renal proximal tubular cells. *Int J Mol Med* **40**:1957-1964.
- Kim JY, Garcia-Carbonell R, Yamachika S, Zhao P, Dhar D, Loomba R, Kaufman RJ, Saltiel AR and Karin M (2018a) ER Stress Drives Lipogenesis and Steatohepatitis via Caspase-2 Activation of S1P. *Cell* **175**:133-145 e115.
- Kim MS, Yoo BC, Yang WS, Han SY, Jeong D, Song JM, Kim KH, Aravinthan A, Kim JH, Kim JH, Kim SC and Cho JY (2018b) Src is the primary target of aripiprazole, an atypical antipsychotic drug, in its anti-tumor action. *Oncotarget* **9**:5979-5992.
- Lang S, Pfeiffer S, Lee PH, Cavalie A, Helms V, Forster F and Zimmermann R (2017) An Update on Sec61 Channel Functions, Mechanisms, and Related Diseases. *Front Physiol* **8**:887.
- Liu J, Ibi D, Taniguchi K, Lee J, Herrema H, Akosman B, Mucka P, Salazar Hernandez MA, Uyar MF, Park SW, Karin M and Ozcan U (2016) Inflammation Improves Glucose Homeostasis through IKKbeta-XBP1s Interaction. *Cell* **167**:1052-1066 e1018.
- Luo B and Lee AS (2013) The critical roles of endoplasmic reticulum chaperones and unfolded protein response in tumorigenesis and anticancer therapies. *Oncogene* **32**:805-818.
- Maurel M, Chevet E, Tavernier J and Gerlo S (2014) Getting RIDD of RNA: IRE1 in cell fate regulation. *Trends Biochem Sci* **39**:245-254.
- McGrath EP, Logue SE, Mnich K, Deegan S, Jager R, Gorman AM and Samali A (2018) The Unfolded Protein Response in Breast Cancer. *Cancers (Basel)* **10**.

- Morlan-Coarasa MJ, Arias-Loste MT, Ortiz-Garcia de la Foz V, Martinez-Garcia O, Alonso-Martin C, Crespo J, Romero-Gomez M, Fabrega E and Crespo-Facorro B (2016) Incidence of non-alcoholic fatty liver disease and metabolic dysfunction in first episode schizophrenia and related psychotic disorders: a 3-year prospective randomized interventional study. *Psychopharmacology (Berl)* **233**:3947-3952.
- Musil R, Obermeier M, Russ P and Hamerle M (2015) Weight gain and antipsychotics: a drug safety review. *Expert Opin Drug Saf* **14**:73-96.
- Nagai G, Mihara K, Nakamura A, Nemoto K, Kagawa S, Suzuki T and Kondo T (2017) Prediction of an Optimal Dose of Aripiprazole in the Treatment of Schizophrenia From Plasma Concentrations of Aripiprazole Plus Its Active Metabolite Dehydroaripiprazole at Week 1. *Ther Drug Monit* **39**:62-65.
- Owen MJ, Sawa A and Mortensen PB (2016) Schizophrenia. *Lancet* **388**:86-97.
- Ozcan U, Cao Q, Yilmaz E, Lee AH, Iwakoshi NN, Ozdelen E, Tuncman G, Gorgun C, Glimcher LH and Hotamisligil GS (2004) Endoplasmic reticulum stress links obesity, insulin action, and type 2 diabetes. *Science* **306**:457-461.
- Panariello F, De Luca V and de Bartolomeis A (2011) Weight gain, schizophrenia and antipsychotics: new findings from animal model and pharmacogenomic studies. *Schizophr Res Treatment* **2011**:459284.
- Pardo V, Gonzalez-Rodriguez A, Muntane J, Kozma SC and Valverde AM (2015) Role of hepatocyte S6K1 in palmitic acid-induced endoplasmic reticulum stress, lipotoxicity, insulin resistance and in oleic acid-induced protection. *Food Chem Toxicol* **80**:298-309.
- Rutkowski DT, Arnold SM, Miller CN, Wu J, Li J, Gunnison KM, Mori K, Sadighi Akha AA, Raden D and Kaufman RJ (2006) Adaptation to ER stress is mediated by differential stabilities of pro-survival and pro-apoptotic mRNAs and proteins. *PLoS Biol* **4**:e374.
- Shemorry A, Harnoss JM, Guttman O, Marsters SA, Komuves LG, Lawrence DA and Ashkenazi A (2019) Caspase-mediated cleavage of IRE1 controls apoptotic cell commitment during endoplasmic reticulum stress. *Elife* **8**.
- Soliman HM, Wagih HM, Algaidi SA and Hafiz AH (2013) Histological evaluation of the role of atypical antipsychotic drugs in inducing non-alcoholic fatty liver disease in adult male albino rats (light and electron microscopic study). *Folia Biol (Praha)* **59**:173-180.
- Tang CH, Ranatunga S, Kriss CL, Cubitt CL, Tao J, Pinilla-Ibarz JA, Del Valle JR and Hu CC (2014) Inhibition of ER stress-associated IRE-1/XBP-1 pathway reduces leukemic cell survival. *J Clin Invest* **124**:2585-2598.
- Taylor CW and Tovey SC (2010) IP(3) receptors: toward understanding their activation. *Cold Spring Harb Perspect Biol* **2**:a004010.
- van Os J and Kapur S (2009) Schizophrenia. *Lancet* **374**:635-645.
- Verfaillie T, Garg AD and Agostinis P (2013) Targeting ER stress induced apoptosis and inflammation in cancer. *Cancer Lett* **332**:249-264.
- Ye J, Rawson RB, Komuro R, Chen X, Dave UP, Prywes R, Brown MS and Goldstein JL (2000) ER stress induces cleavage of membrane-bound ATF6 by the same proteases that process SREBPs. *Mol Cell* **6**:1355-1364.
- Yoo S, Kim MY and Cho JY (2018) Syk and Src-targeted anti-inflammatory activity of aripiprazole, an atypical antipsychotic. *Biochem Pharmacol* **148**:1-12.
- Yoshida H, Matsui T, Yamamoto A, Okada T and Mori K (2001) XBP1 mRNA is induced by ATF6 and spliced by IRE1 in response to ER stress to produce a highly active transcription factor. *Cell* **107**:881-891.
- Zeeshan HM, Lee GH, Kim HR and Chae HJ (2016) Endoplasmic Reticulum Stress and Associated ROS. *Int J Mol Sci* **17**:327.
- Zhang K and Kaufman RJ (2008) From endoplasmic-reticulum stress to the inflammatory response. *Nature* **454**:455-462.

## Footnotes

The authors declare no financial conflict of interest. Research was funded by grants from the David R. Bloom Center for Pharmacy, the Dr. Adolph and Klara Brettler Center for Research in Pharmacology. FF, PD and VF are Marie Curie fellows [Treatment H2020-MSCA-ITN-721236]. AMV, PR and IGM were supported by grants [RTI2018-094052-B-100] (MCIU/AEI/FEDER, UE)) and [S2017/BMD-3684] MOIR2-CM (Comunidad de Madrid, Spain) and CIBERdem (ISCIII, Spain).

## Legends for figures

**Figure 1: Aripiprazole, but not Olanzapine, induces ER stress in HepG2 cells.** A. HepG2 cells were treated overnight with the indicated concentrations of Ari. Total cell extracts of the adhered cells were analysed by immunoblotting for phospho-IRE1, total IRE1, total PERK and p97 as loading control. The lower panel shows RT-PCR analysis of XBP1 splicing following Ari treatment. A representative experiment of three independent repetitions is shown. B. Relative quantification of phospho IRE1 (24h). Shown is an average of three independent experiments  $\pm$  SD. C. Time course of IRE1 phosphorylation following Ari treatment. Thapsigargin (Tg, 2.5  $\mu$ g/ml) was used as a positive control. D. Similar analysis as in A was conducted for Ola. Statistical significance is indicated by  $**p < 0.01$ , and  $***p < 0.001$  by ANOVA.

**Figure 2: Aripiprazole promotes immobilization of calcium to the cytoplasm.** A. The time line of the experimental procedure. Tg is used twice as a positive control and to release ER calcium storage immediately before imaging. B. Pseudo-colored images of calcium concentrations of HepG2 cells before ('basal') and after Tg (2.5  $\mu$ g/ml) application to release the ER calcium storages following overnight treatment with DMSO as a negative control, Tg (2.5  $\mu$ g/ml) as a positive control or Ari. Scale bar indicates levels of intracellular calcium. C. Changes of intracellular calcium levels in HepG2 cells treated as shown in A. Statistical significance is indicated by  $*p < 0.05$ , of at least 5 independent measurements by ANOVA.

**Figure 3: IRE1 contributes more than PERK to Ari-induced cytotoxicity.** A. WT, IRE1 KO and PERK KO HepG2 were treated with DMSO and 30  $\mu$ M Ari. Cells were stained with PI and analysed by flow cytometry. Representative dot plots of forward versus side scattering properties and percentage of PI-positive cells are shown. B. Percentage of propidium iodide (PI) positive cells, measured by flow cytometry, following overnight treatment with DMSO, Ari (30  $\mu$ M) and Ari with Z-VAD-FMK (25  $\mu$ M). Average of three independent experiments  $\pm$  SD is shown. Statistical significance is indicated by  $*p < 0.05$  and  $**p < 0.01$  by ANOVA for Z-VAD-FMK treatment and for the KO cells by paired Student's *t* test).

**Figure 4: NAC, BAPTA-AM and EGTA do not protect from Aripiprazole-induced cell death.** A. HepG2 cells were treated overnight with DMSO and 30  $\mu$ M Ari in the absence or

presence of NAC, BAPTA-AM or EGTA. Percentage of PI positive cells of a representative experiment, as measured by flow cytometry following treatment, is shown. B. Average of three independent experiments  $\pm$  SD is shown. No statistical significance was measured.

**Figure 5: GSH ethyl ester protects from Aripiprazole-induced cell death.** HepG2 cells were treated overnight with DMSO and 30  $\mu$ M Ari in the absence or presence of GSH ethyl ester. Percentage of PI positive cells of a representative experiment, as measured by flow cytometry following treatment, is shown. Average of three independent experiments  $\pm$  SD is shown. Statistical significance is indicated by \*  $p < 0.05$  by ANOVA.

**Figure 6: Aripiprazole induces ER stress, accumulation of lipids and calcium mobilization from the ER in primary mouse hepatocytes.** A and B. Primary mouse hepatocytes were isolated and treated with Ari at different concentrations. 4 h (A) and 8 h (C) after exposure to the drug cells were lysed and analysed by immunoblotting for phospho IRE1, total IRE1, total PERK and p97 as loading control. 4h (B) and 8h (D) Relative quantification of phospho IRE1. Shown is an average of three independent experiments  $\pm$  SD. E. RT-PCR analysis for XBP1 mRNA splicing following Ari treatment. Tunicamycin (Tm) (2.5  $\mu$ g/ml) was used as a positive control for ER stress induction. F. Oil Red-O staining of primary mouse hepatocytes following 24h treatment with DMSO, Tm (2.5  $\mu$ g/ml) or 30  $\mu$ M Ari. Representative phase contrast images are shown. G Pseudo-colored images of calcium concentrations of Primary Hepatocytes before ('Basal') and after Tg(2,5  $\mu$ g/ml) application to release the ER calcium storages following overnight treatment with DMSO as a negative control, Tg (2.5  $\mu$ g/ml) as a positive control or 30  $\mu$ M Ari. Scale bar indicates levels of intracellular calcium. H. Changes of intracellular calcium levels in Primary Hepatocytes treated as shown in G. Statistical significance is indicated by \*\* $p < 0.01$  by ANOVA

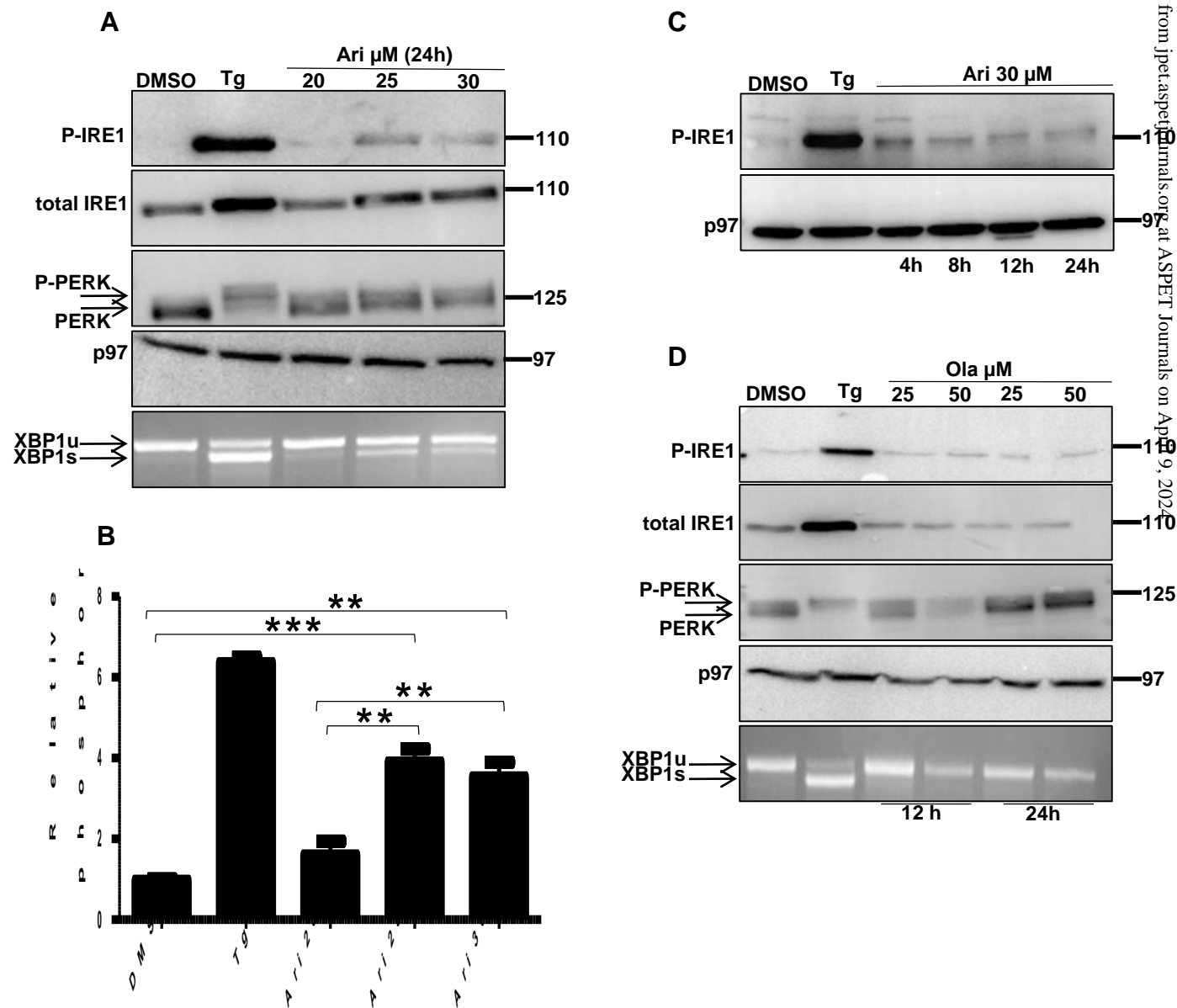


Figure 1

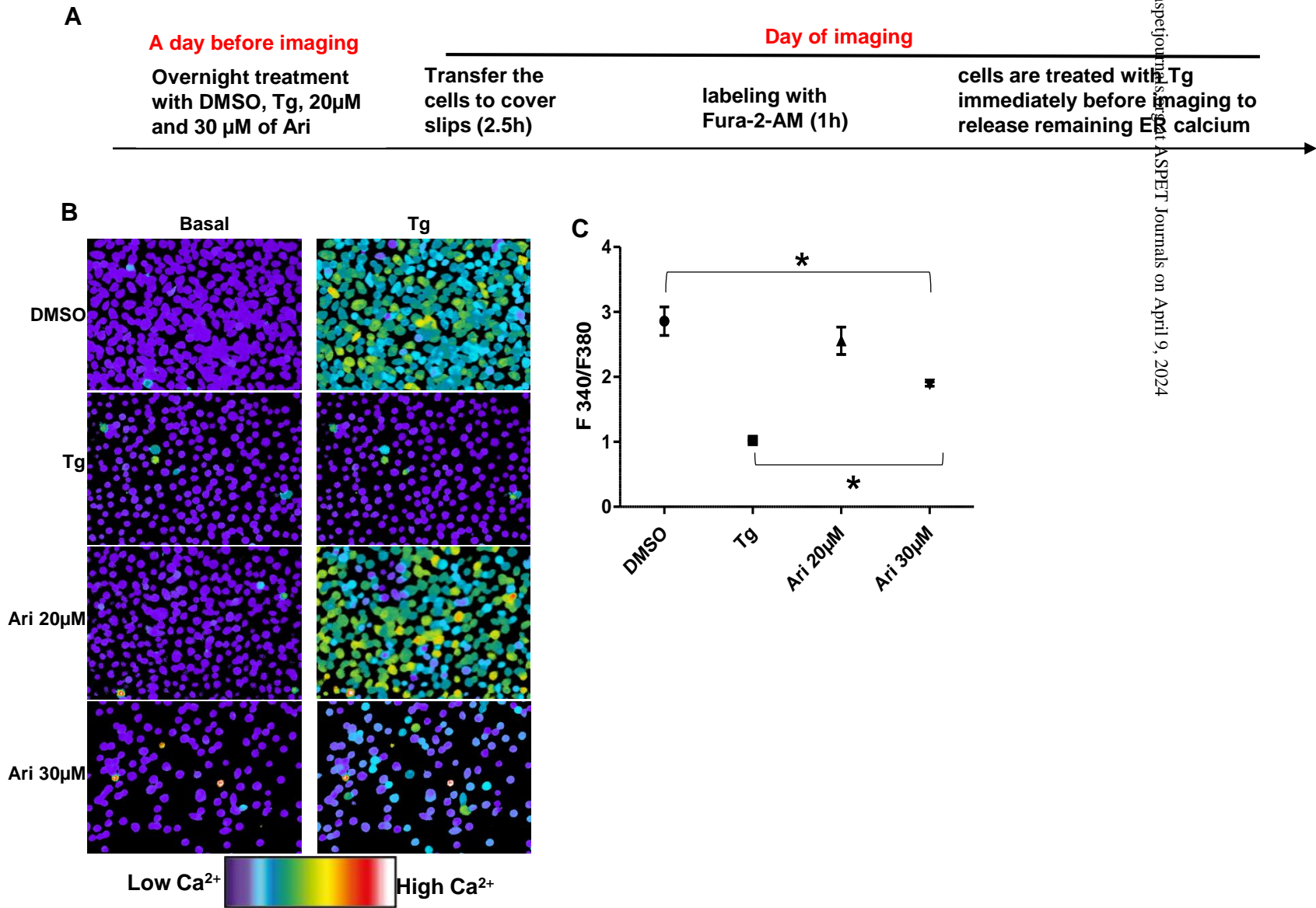
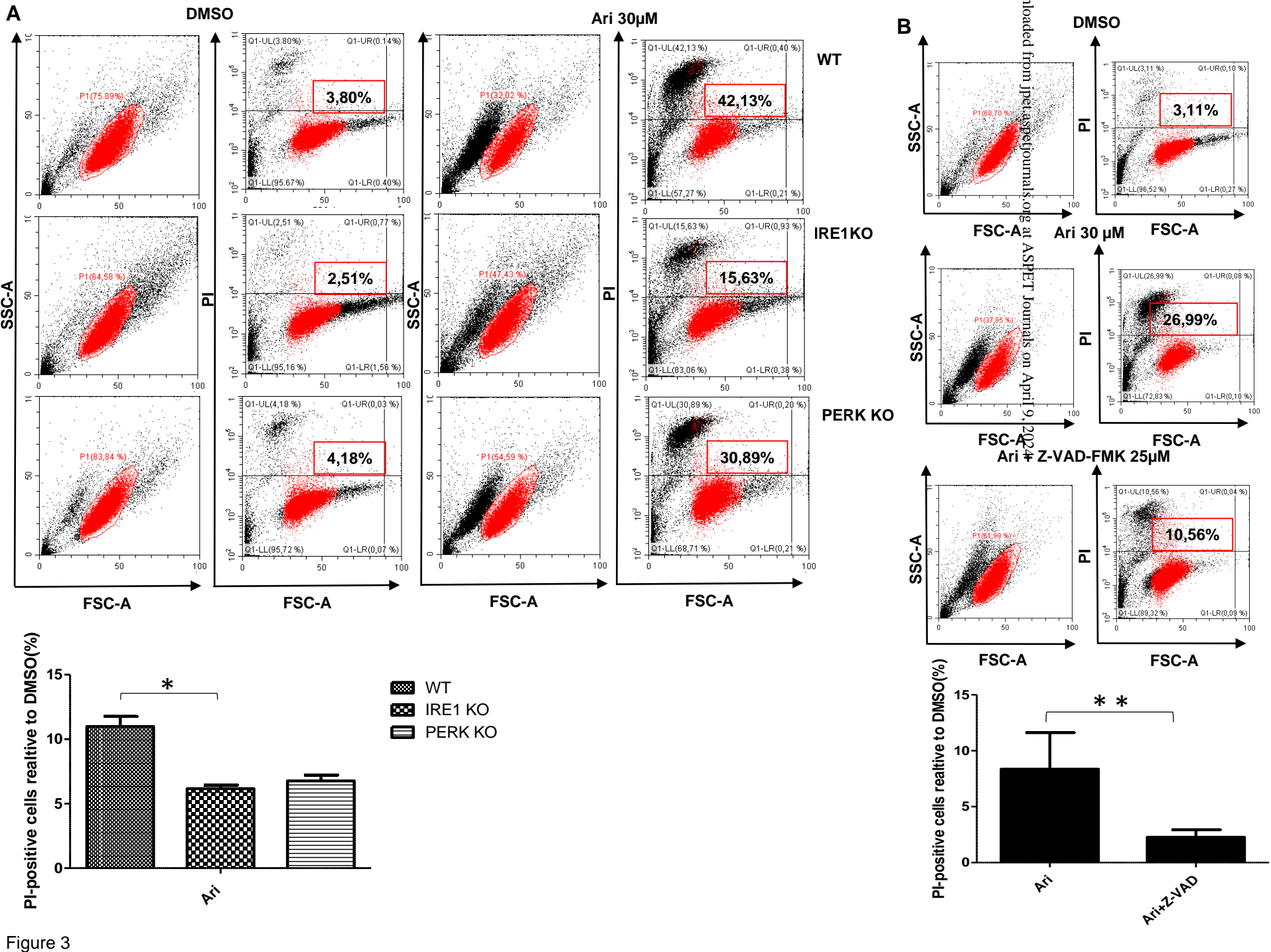


Figure 2



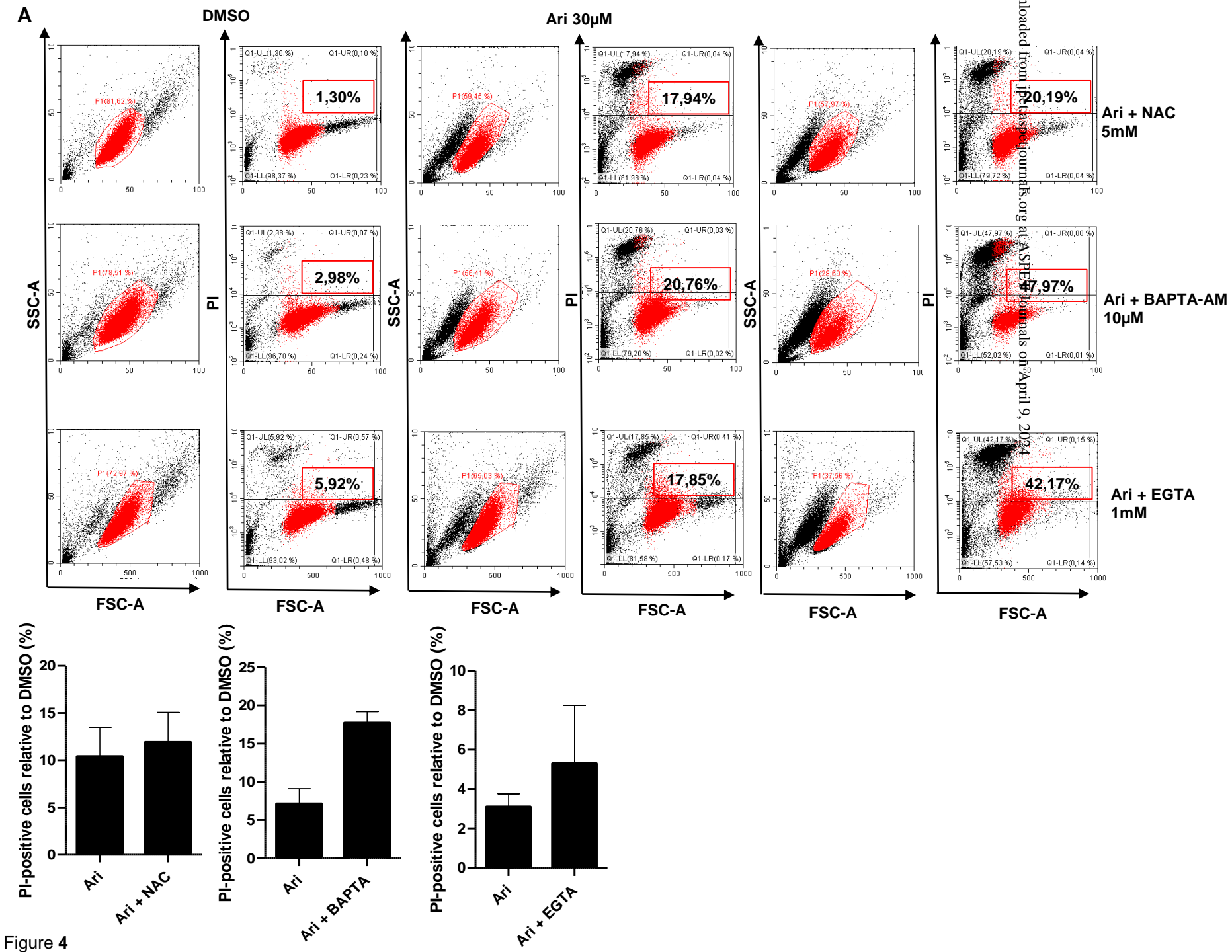


Figure 4

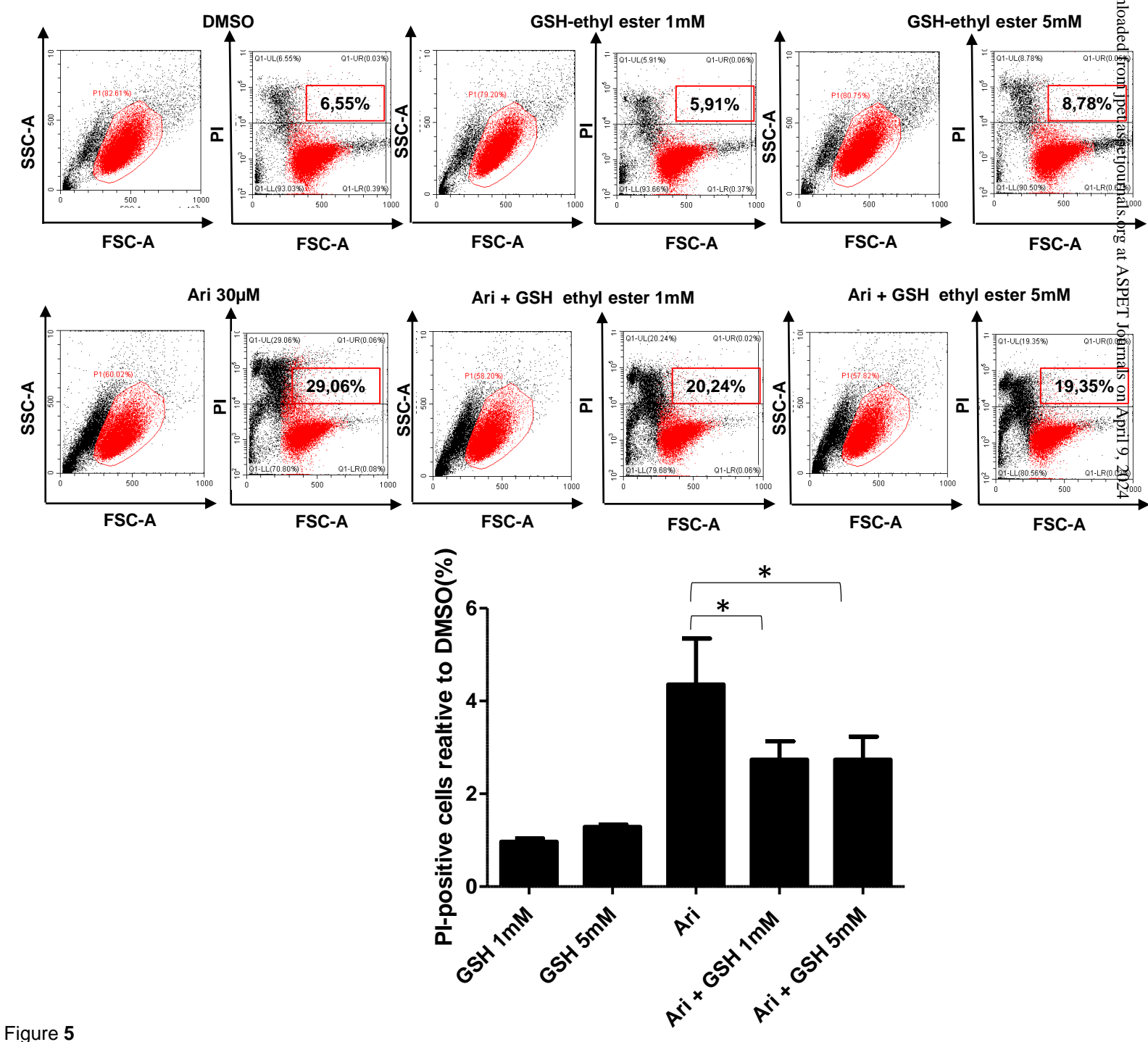


Figure 5

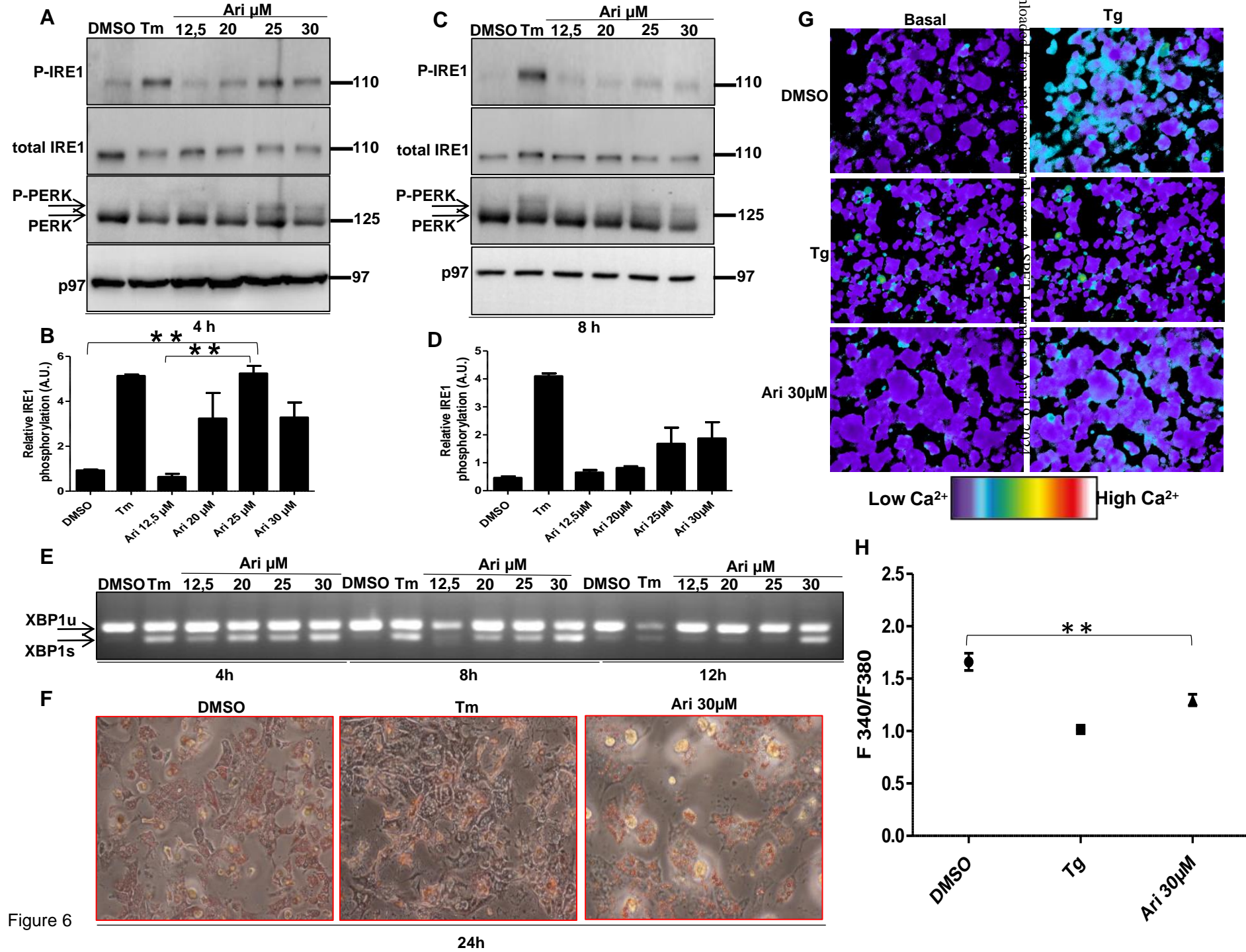


Figure 6

**Supplemental data for JPET #264481**

**Aripiprazole cytotoxicity coincides with activation of the unfolded protein response in human hepatic cells**

**Authors:**

**Francesca Forno<sup>1</sup>, Yossi Maatuf<sup>1</sup>, Shatha Boukeileh<sup>1</sup>, Priya Dipta<sup>1</sup>, Mohamed Mahameed<sup>1</sup>, Odai Darawshi<sup>1</sup>, Vitor Ferreira<sup>2,3</sup>, Patricia Rada<sup>2,3</sup>, Irma García-Martínez<sup>2,3</sup>, Einav Gross<sup>4</sup>, Avi Priel<sup>1</sup>, Ángela M. Valverde<sup>2,3</sup>, Boaz Tirosh<sup>1</sup>**

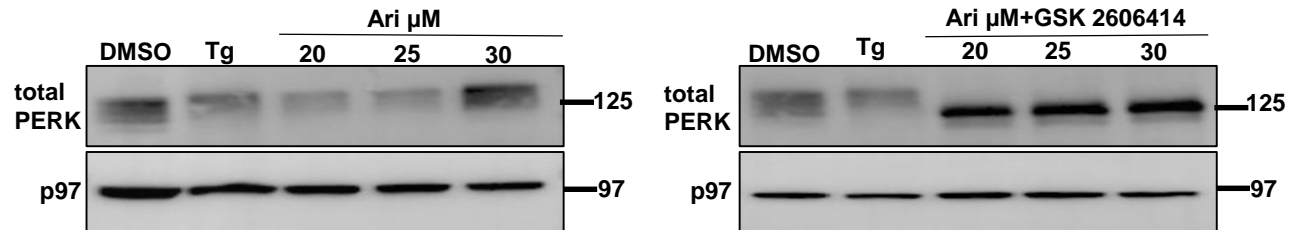
**Affiliations:**

<sup>1</sup>Institute for Drug Research, School of Pharmacy, Faculty of Medicine, Hebrew University of Jerusalem, Jerusalem, Israel

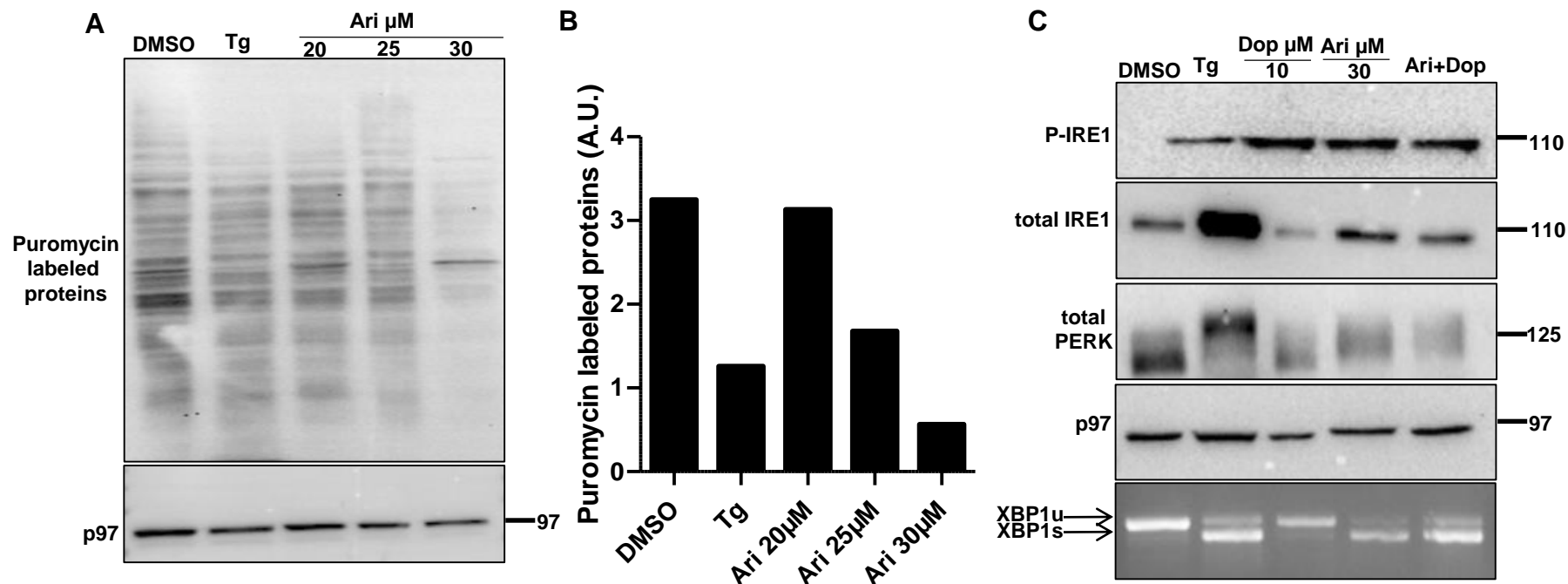
<sup>2</sup>Instituto de Investigaciones Biomédicas Alberto Sols (CSIC-UAM), 28029, Madrid, Spain

<sup>3</sup>Centro de Investigación Biomédica en Red de Diabetes y Enfermedades Metabólicas Asociadas (CIBERdem), ISCIII, 28029, Madrid, Spain

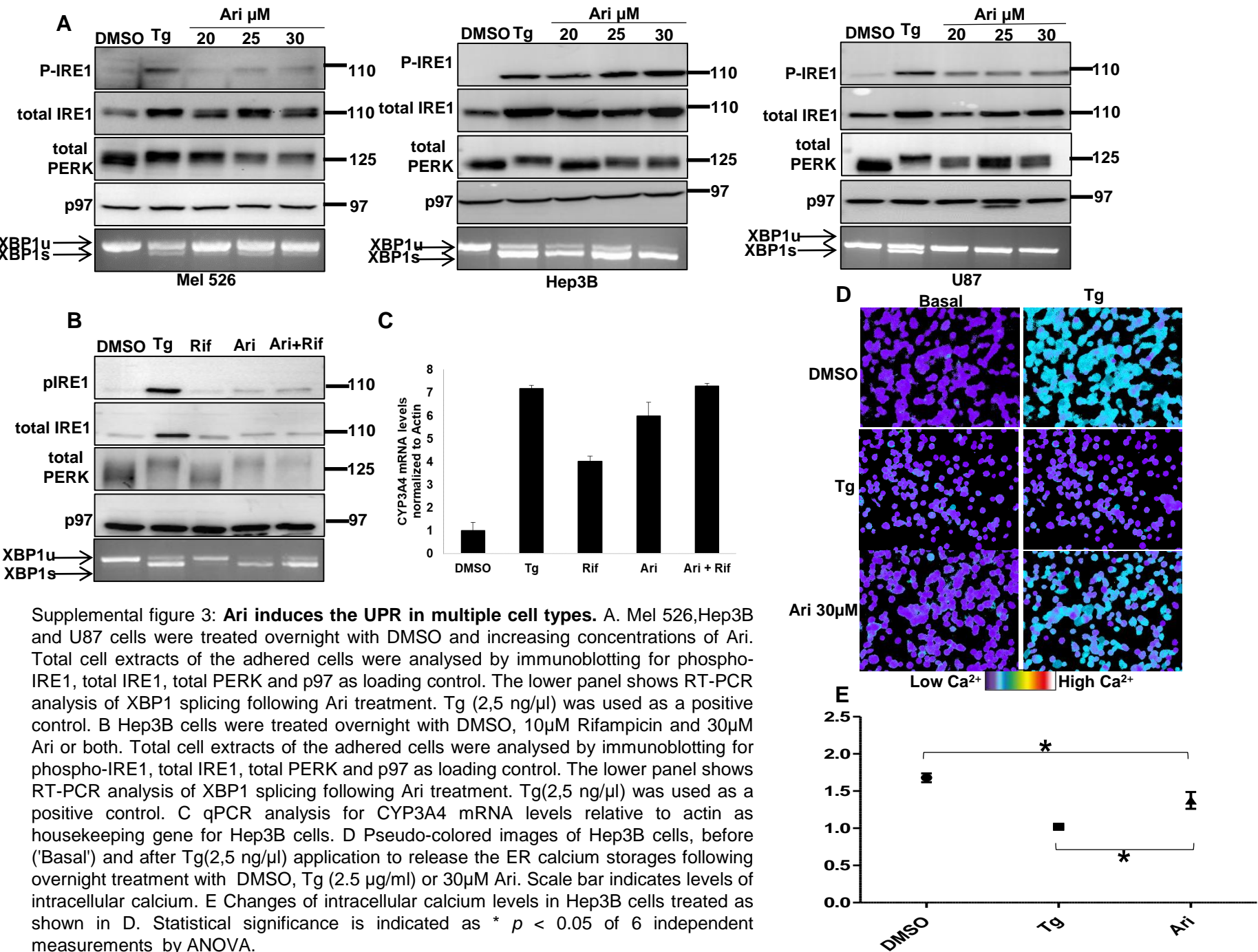
<sup>4</sup>Dept. of Biochemistry and Molecular Biology, IMRIC, Faculty of Medicine, The Hebrew University of Jerusalem, Ein Kerem. P.O. Box 12271, Jerusalem, 9112102, Israel



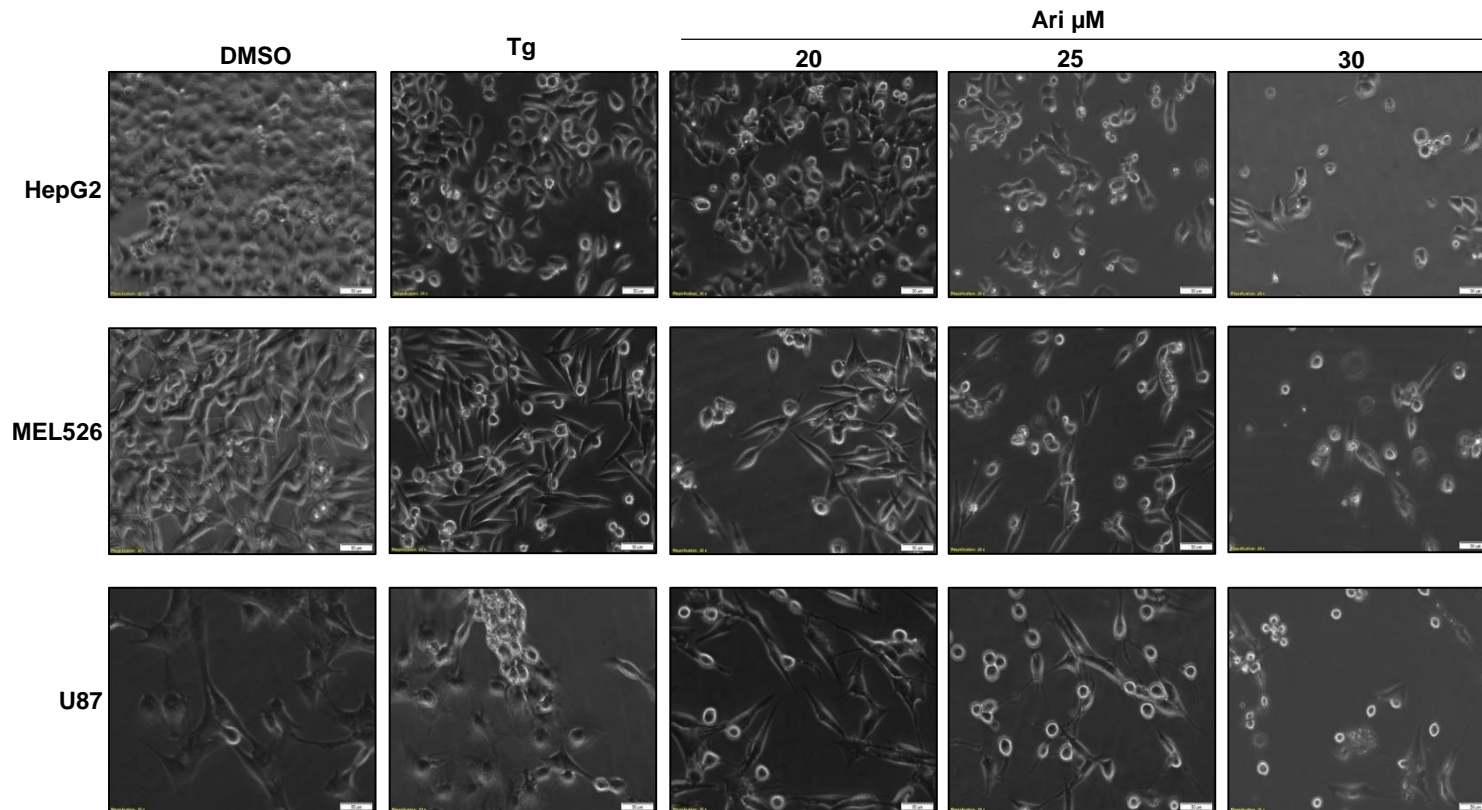
Supplemental figure 1: **Addition of the PERK inhibitor GSK 2606414 reverses Ari-induced PERK phosphorylation.** HepG2 cells were incubated overnight with DMSO and increasing concentrations of Ari +/- PERK inhibitor GSK 2606414 (500nM). Total cell extracts of the adhered cells were analysed by immunoblotting for total PERK and p97 as loading control. Tg (2.5  $\mu$ g/ml) was used as a positive control.



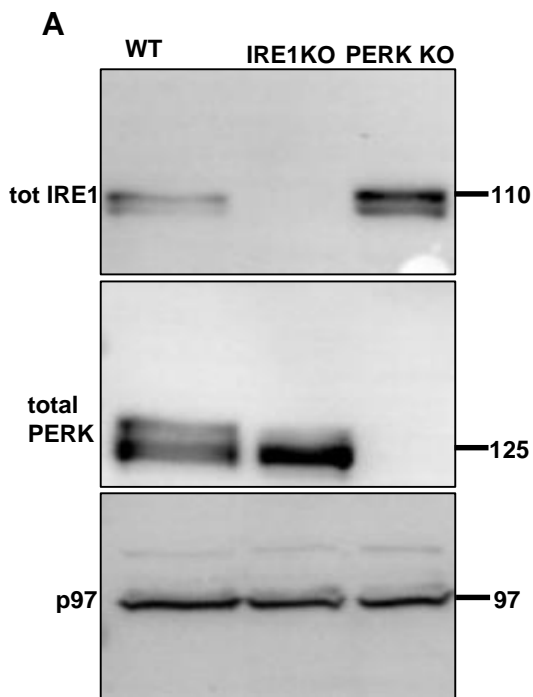
Supplemental figure 2: **Ari induces the UPR in a dopamine independent manner.** A. HepG2 cells were incubated overnight with DMSO and increasing concentrations of Ari. Cells were harvested, centrifuged, and resuspended in fresh medium, then pulsed for 10 min by adding of puromycin to a final concentration of 0,1 mg/ml. Following the addition of puromycin, cells were immediately incubated at 37°C under 300 rpm shaking and ice-cold PBS was added to a volume of 40mL to terminate the protein labeling. Cells were washed twice with cold PBS and lysed in 200  $\mu$ l of 1 x reduced Laemmli sample buffer preheated to 70°C. Equal volumes were loaded on 12 % SDS–PAGE and following blotting, probed with anti-puromycin antibody and p97 as loading control. Tg(2,5 ng/ $\mu$ l) was used as a positive control. B. Quantification of puromycin-labeled proteins relative to p97. C. HepG2 cells were treated overnight with DMSO, 10 $\mu$ M Dopamine and 30 $\mu$ M Ari or both. Total cell extracts of the adhered cells were analysed by immunoblotting for phospho-IRE1, total IRE1, total PERK and p97 as loading control. The lower panel shows RT-PCR analysis of XBP1 splicing following Ari treatment. Tg(2,5 ng/ $\mu$ l) was used as a positive control.



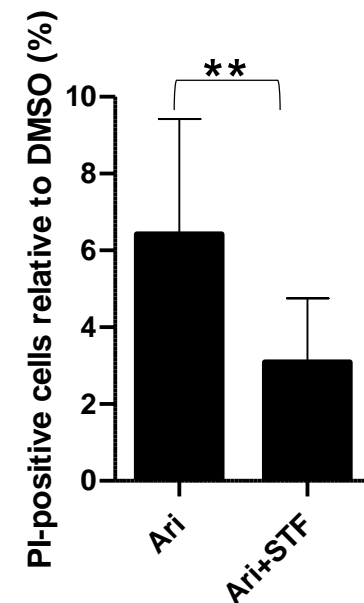
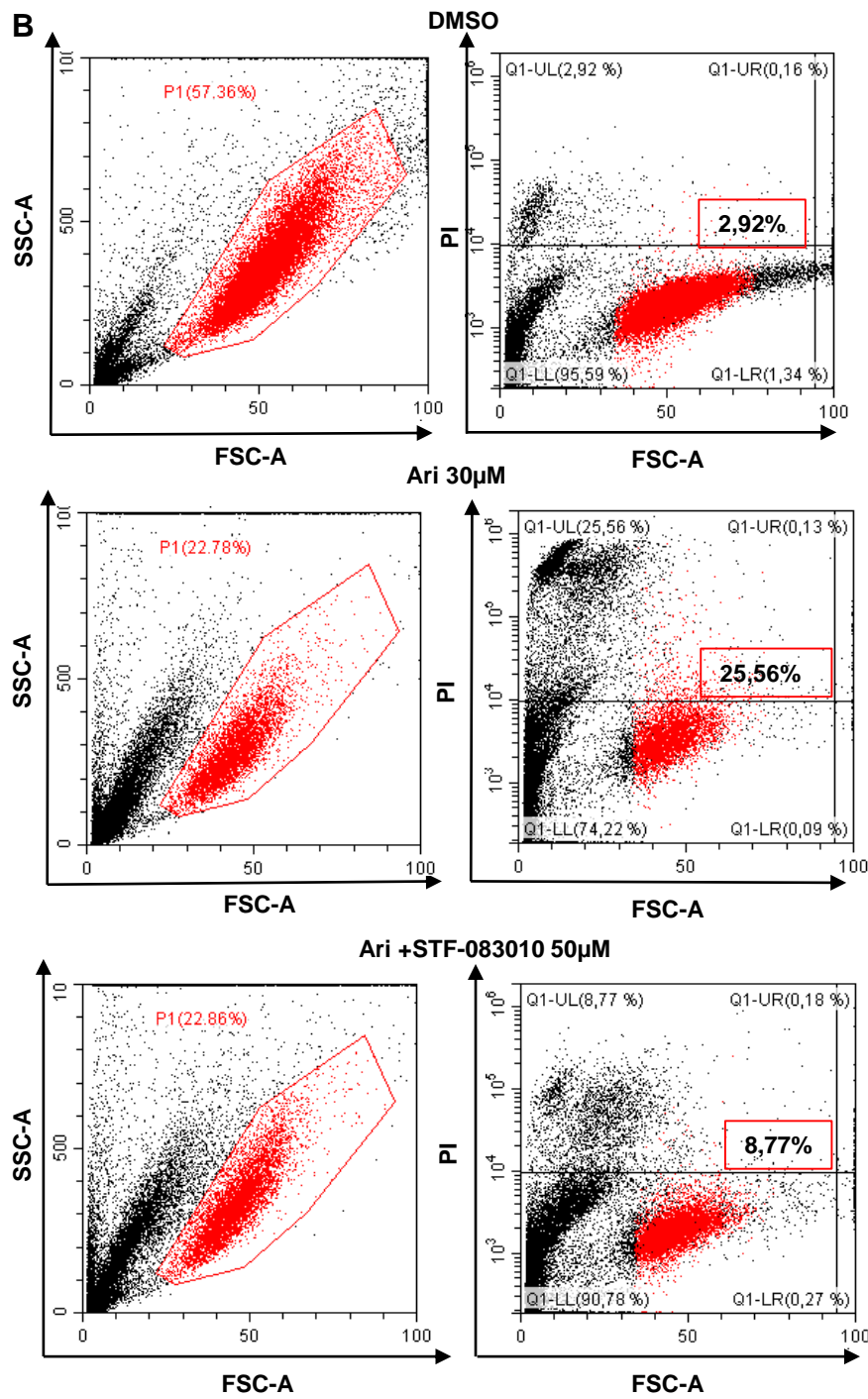
Supplemental figure 3: **Ari induces the UPR in multiple cell types.** A. Mel 526, Hep3B and U87 cells were treated overnight with DMSO and increasing concentrations of Ari. Total cell extracts of the adhered cells were analysed by immunoblotting for phospho-IRE1, total IRE1, total PERK and p97 as loading control. The lower panel shows RT-PCR analysis of XBP1 splicing following Ari treatment. Tg (2,5 ng/ $\mu$ l) was used as a positive control. B Hep3B cells were treated overnight with DMSO, 10 $\mu$ M Rifampicin and 30 $\mu$ M Ari or both. Total cell extracts of the adhered cells were analysed by immunoblotting for phospho-IRE1, total IRE1, total PERK and p97 as loading control. The lower panel shows RT-PCR analysis of XBP1 splicing following Ari treatment. Tg (2,5 ng/ $\mu$ l) was used as a positive control. C qPCR analysis for CYP3A4 mRNA levels relative to actin as housekeeping gene for Hep3B cells. D Pseudo-colored images of Hep3B cells, before ('Basal') and after Tg (2,5 ng/ $\mu$ l) application to release the ER calcium storages following overnight treatment with DMSO, Tg (2.5  $\mu$ g/ml) or 30 $\mu$ M Ari. Scale bar indicates levels of intracellular calcium. E Changes of intracellular calcium levels in Hep3B cells treated as shown in D. Statistical significance is indicated as \*  $p < 0.05$  of 6 independent measurements by ANOVA.

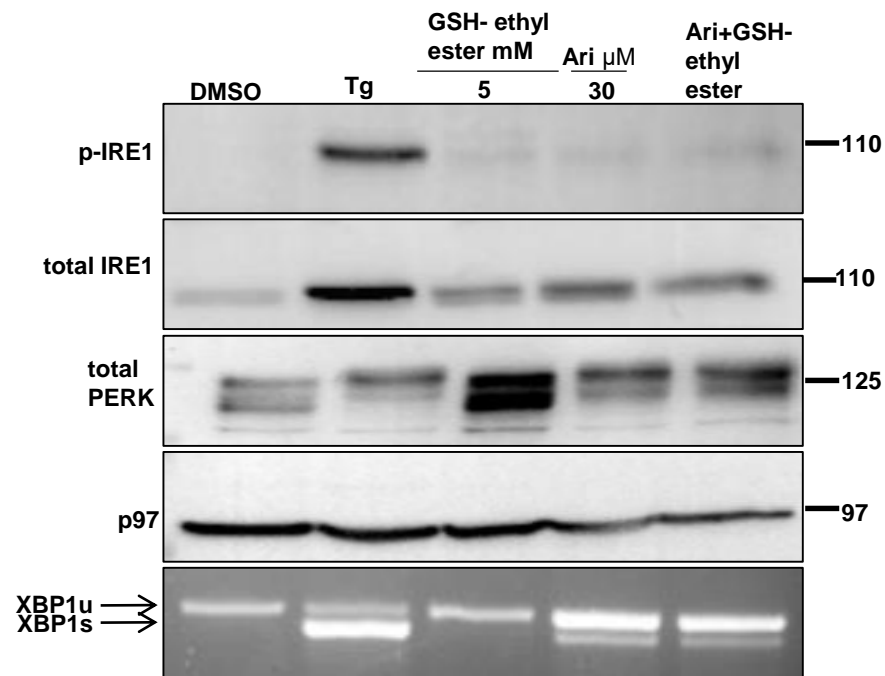


Supplemental figure 4: **Cytotoxicity of Ari coincides with the concentrations that induce the UPR.** HepG2, Mel 526 and U87 cells were treated overnight with DMSO, Tg(2,5 ng/ $\mu$ l) and increasing concentrations of Ari, then light images of cells were taken using Nomarsky interference contrast microscopy.

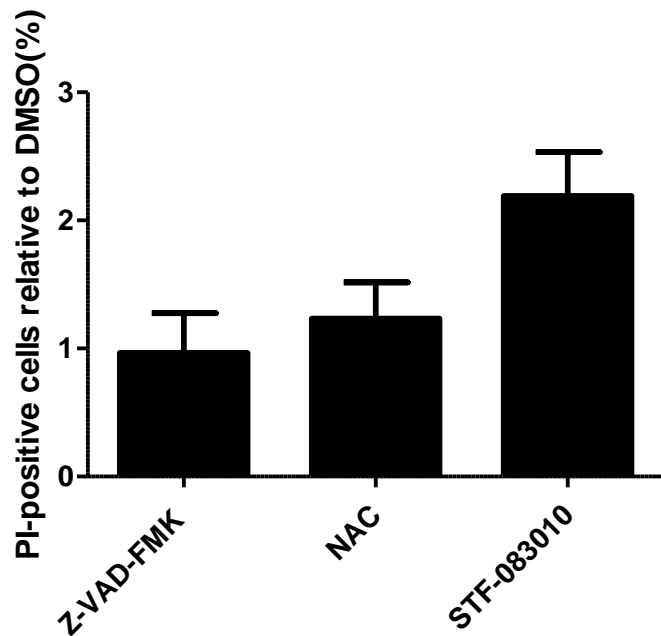
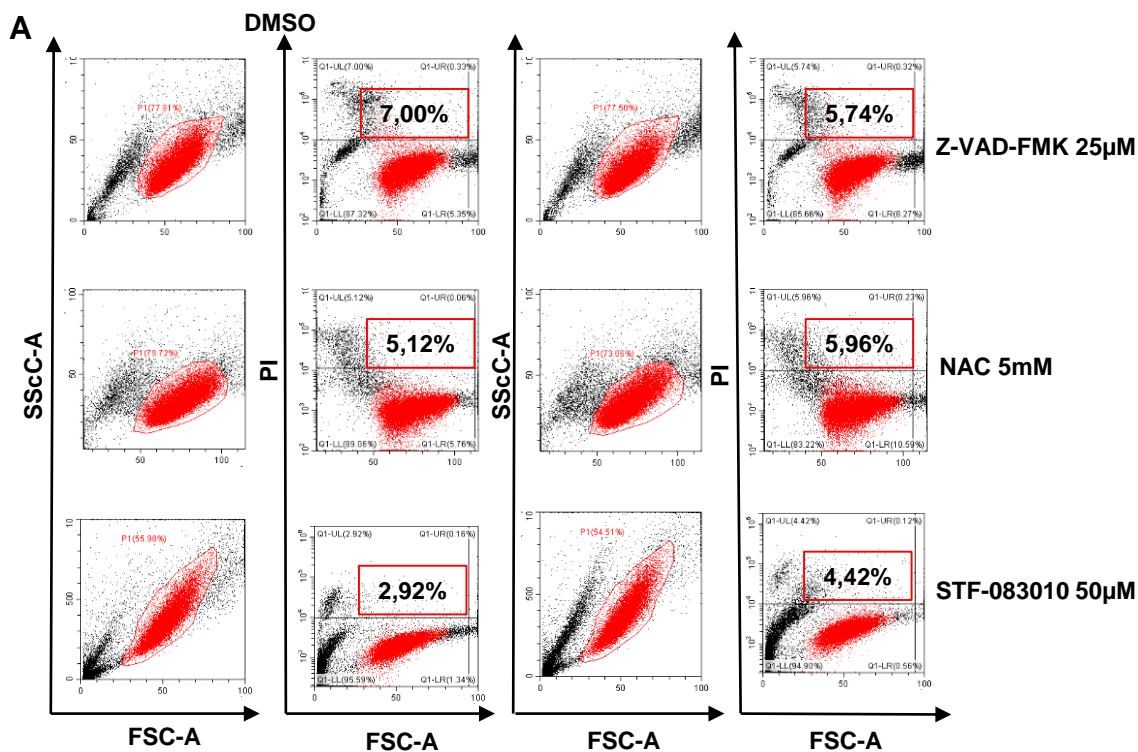


Supplemental figure 5: **Inhibition of IRE1 inhibits Ari cytotoxicity in melanoma cells.** A. Immunoblotting of total IRE1, total PERK and p97 as loading control in HepG2 cells following CRISPR/Cas9 deletion. B. Melanoma 526 cells were treated with Aripiprazole in the presence and absence of the IRE1 inhibitor STF-083010. Percentage of propidium iodide (PI) positive cells, measured by flow cytometry, following overnight treatment with DMSO, 30 $\mu$ M Ari and Ari with 50 $\mu$ M STF-083010. C Shown is the average of three independent experiments  $\pm$  SD. Statistical significance is indicated as \*\*P < 0.01 (ANOVA followed by a multiple comparison test).

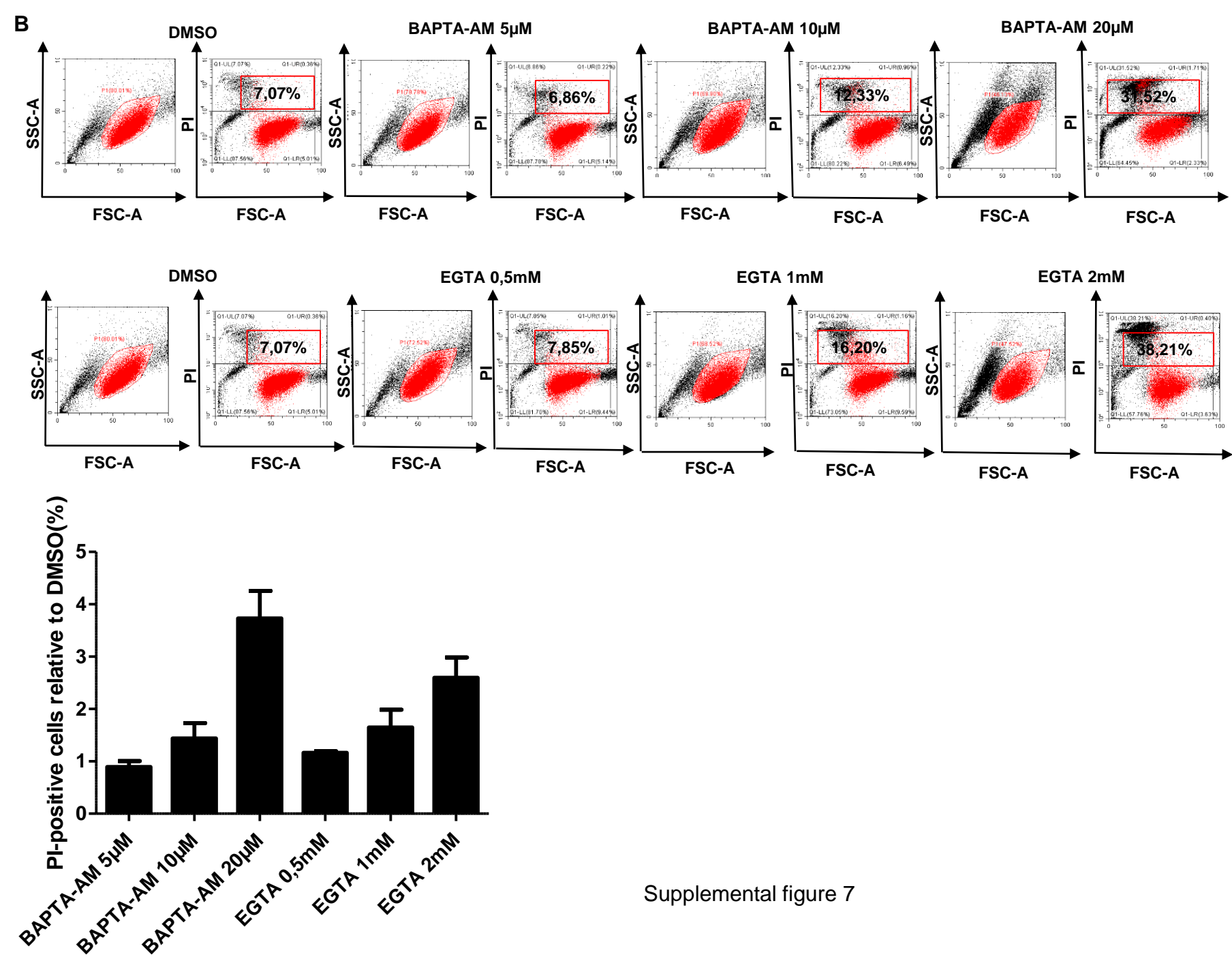




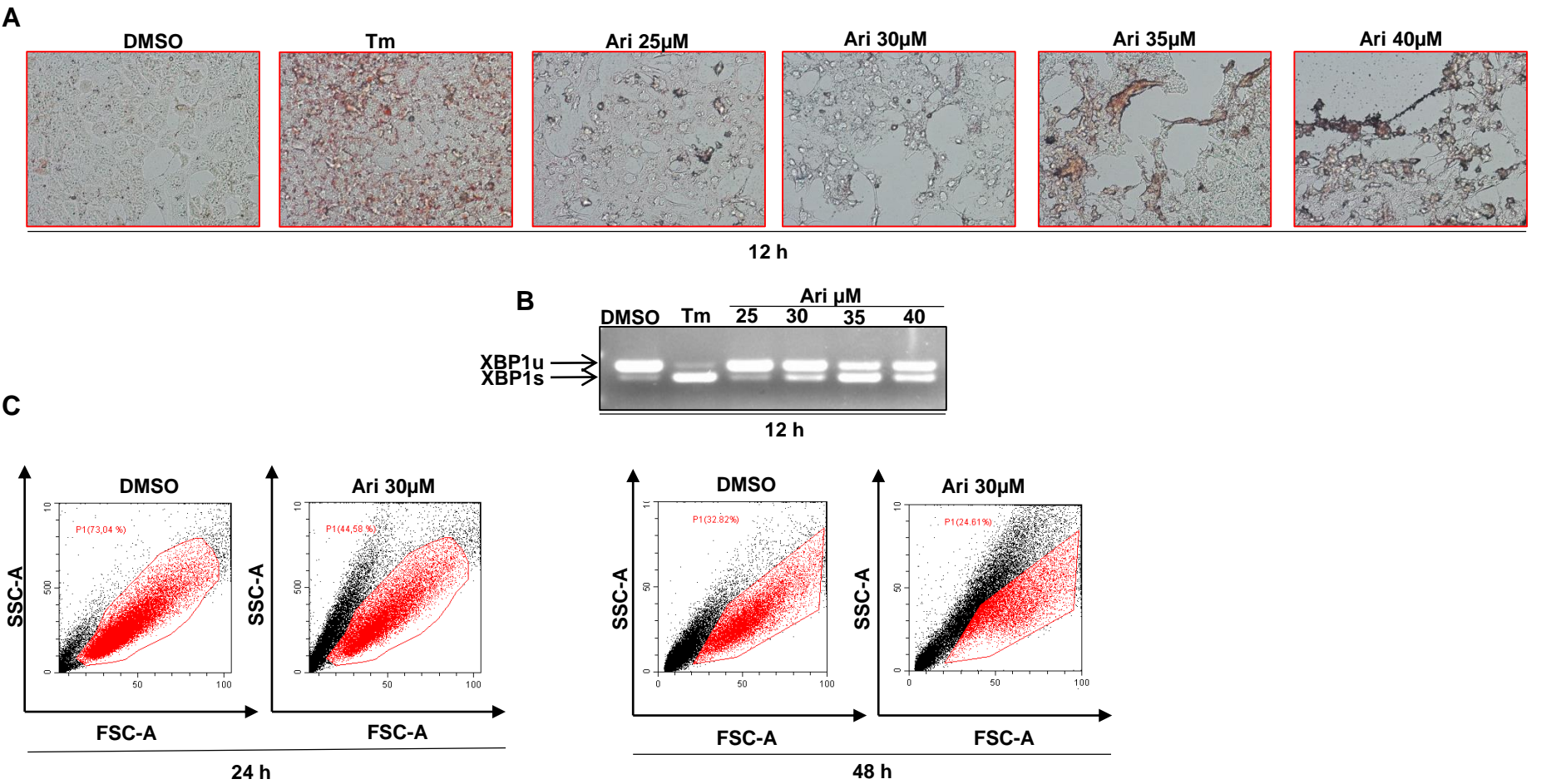
Supplemental figure 6: **GSH-ethyl ester does not prevent HepG2 cells from Ari-induced ER stress.** HepG2 cells were treated overnight with DMSO, 5mM GSH-ethyl ester and 30μM Ari or both. Total cell extracts of the adhered cells were analysed by immunoblotting for phospho-IRE1, total IRE1, total PERK and p97 as loading control. The lower panel shows RT-PCR analysis of XBP1 splicing following Ari treatment. Tg(2,5 ng/μl) was used as a positive control.



Supplemental figure 7: **Z-VAD-FMK, NAC and STF083010 are not toxic, but BAPTA-AM and EGTA induced toxicity in HepG2 cells in a dose-dependent manner.** A. Percentage of propidium iodide (PI) positive cells, measured by flow cytometry, following overnight treatment with DMSO, Z-VAD-FMK 25μM, NAC 5mM and STF-083010 50μM. Shown is the average of three independent experiments ± SD. B Percentage of propidium iodide (PI) positive cells, measured by flow cytometry, following overnight treatment with DMSO, increasing concentrations of BAPTA and increasing concentrations of EGTA. Shown is the average of three independent experiments ± SD.



Supplemental figure 7



Supplemental figure 8: **Development of ER stress coincides with intracellular lipid accumulation** A Oil-Red-O staining of primary mouse hepatocytes following 12h treatment with DMSO, Tunicamycin (2.5 ng/ $\mu$ l) or increasing concentrations of Ari. Representative phase contrast images are shown. B. RT-PCR analysis of XBP1 splicing following Ari treatment. Tm (2.5 ng/ $\mu$ l) was used as a positive control. C. Flow cytometry of primary hepatocytes after 24 and 48h of treatment. Live cells are gated in red.